Engineering Structures 275 (2023) 115234

Contents lists available at ScienceDirect

Engineering Structures

journal homepage: www.elsevier.com/locate/engstruct

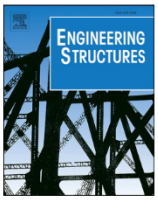

Characterisation of mortarless refractory masonry joints under elevated temperatures

Pratik N. Gajjar [a,*], Pieter Put [b], João M. Pereira [a], Bruno Luchini [b], Sido Sinnema [b], Paulo B. Lourenço [a]

[a] University of Minho, ISISE, Department of Civil Engineering, Guimarães, Portugal
[b] Ceramics Research Centre, Tata Steel, 1951MD Velsen Noord, The Netherlands

ARTICLE INFO

Keywords:
Masonry
Refractories
Mortarless masonry
Dry joint
Joint behaviour
High temperature

ABSTRACT

Refractory linings are commonly employed in Industrial vessels used in high-temperature processes to protect them against extreme working environments. The working lining of an industrial steel ladle frequently employs mortarless refractory masonry to contain the molten steel and limit heat losses. Such masonry lining undergoes high thermomechanical loads, primarily due to thermal expansion arising from thermal and mechanical boundary conditions. Dry joints, described as a physical break in the continuum, reduce some of these effects. Therefore, understanding dry joints is an essential factor for developing numerical constitutive models that employ a meso or macro modelling approach. This work aims to experimentally investigate the normal compressive behaviour of dry joints in refractory masonry. For this purpose, various refractory specimens of alumina-spinel material are tested from ambient temperature to 1200 °C. The results obtained from these experiments are then used to identify critical joint parameters with different mathematical models for the interface. The outcome describes exponential joint closing behaviour with respect to the force applied. It was observed that the pressure required to close a joint reduces with an increase in temperature. The exponential model was then used to numerically simulate the joint closure of mortarless refractory masonry. Finally, numerical and experimental results were compared.

1. Introduction

Masonry is a widespread structural element that is being employed in various construction projects. The composition of units (bricks, stones, and refractory materials) and joints (mortar or mortarless) defines masonry. Mortarless masonry (also known as dry-stacked masonry) is present in a wide range of applications, from historical to modern industrial structures. Masonry as refractory linings is frequently found in industrial vessels used in high-temperature processes to ensure protection against the material they contain [1–4]. One of the best examples is the steel ladle, where the refractory masonry is subjected to an extreme environment with high thermal and mechanical loads. The refractory working lining of an industrial steel ladle frequently employs mortarless refractory masonry to contain the molten steel and limit heat losses [5,6]. It can experience temperatures up to 1650 °C during thermal loading due to the storage of molten steel [7].

The configuration of a mortarless refractory lining in an industrial steel ladle is illustrated in Fig. 1. A working lining is built from many individual tapered bricks. This lining undergoes high thermomechanical loads during this operational condition resulting from the combined effects of thermal shocks and mechanical and thermal constraints [8]. The thermal shocks are induced when the molten steel is introduced into the ladle, which also applies ferrostatic pressure to the working lining. However, this ferrostatic pressure is marginal when compared to the stresses induced by the thermal loads. Thermal constraints are generated due to thermal expansion, thermal gradient within the brick and the restraining effect of the outer steel shell. Under such service conditions, refractories may exhibit elastic and inelastic behaviour that is dependent on the duration and magnitudes of the thermal and mechanical loads and the materials' properties. Plasticity and visco-plasticity effects at higher temperatures are attributed to the inelastic behaviour of refractory, which is responsible for the irreversible deformation of the material and consequently to the overall behaviour of the structure [9]. Such loading and restraining conditions can generate normal

* Corresponding author.
E-mail address: pratik.gajjar@civil.uminho.pt (P.N. Gajjar).

https://doi.org/10.1016/j.engstruct.2022.115234
Received 17 June 2022; Received in revised form 30 September 2022; Accepted 30 October 2022

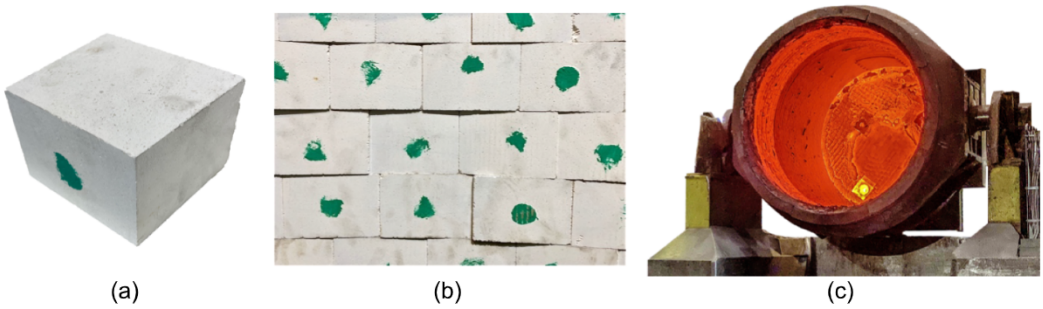

Fig. 1. Mortarless masonry structure: a) refractory brick in trapezoidal shape; b) arrangement of trapezoidal bricks to form a wall; c) application of mortarless masonry in industrial steel ladle during service.

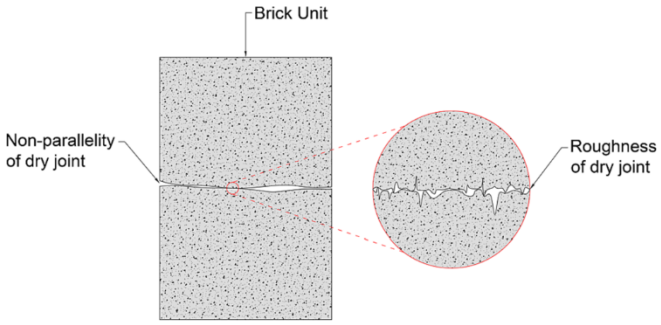

Fig. 2. Graphical representation of dry-joint presenting non-parallelity and surface roughness (not to scale).

compressive stresses in the ranges of 25–60 MPa at various parts of the refractory lining and the experimental studies on refractory masonry walls are often used to create such conditions and validate the numerical models [10,11]. Direct contact between the bricks' surfaces defines a dry joint in masonry. This joint provides a physical break in the continuous media that reduces the global stiffness of the masonry, thus assisting to reduce the stress build-up. Therefore, characterisation of the dry joint is an essential step to understand its global behaviour.

The behaviour of dry joints under normal compressive stress is of fundamental importance to the study of the mechanical behaviour of mortarless masonry. The aperture distribution of joints, contact area distribution and spatial connectivity of the bricks are the main factors that govern the dry joint behaviour [6,12,13]. It is also generally understood that the mechanical behaviour of mortarless masonry is dominated by the deformation of the dry joints [2,5,7,14].

The most fundamental properties of the bounding surfaces of dry joints affecting the joint closure include the material type, contact area distribution, and the spatial and size distributions of the asperities on the surfaces (Fig. 2) [12]. Surface roughness is generated as a part of the manufacturing process or due to manual cutting of the brick. Geometric tolerances primarily appear due to manufacturing tolerances and non-parallelity of the surfaces during construction. These surface asperities gradually close once the normal compressive force is applied. Smaller asperities (rough surfaces in initial contact) close during the initial phase. Progressively, the more significant gaps (surface non-parallelity) close, reducing the effective joint thickness.

Despite the wide use of mortarless masonry and the complex behaviour of dry joints under normal compressive stress, limited experimental research is available on this topic in the literature. Gasser et al. [15] performed an experimental study to evaluate the behaviour of refractory bricks with dry joints at ambient temperature. The study concluded that the joint behaviour could be categorised into two steps, a nonlinear part corresponding to the joint closure and a linear part attributed to the bricks' behaviour (i.e., joint fully closed). The study also found that the joint closure is affected by the surface roughness and the brick shape imperfections such as unevenness of the faces. Andreev et al. [13] evaluated the compressive behaviour of refractory prisms of magnesia-carbon and magnesia-chromite bricks at various temperatures. The study observed an exponential form of joint closure due to the gradual crushing of initially non-parallel surfaces of the specimens. However, the presented experimental work did not evaluate the joint opening behaviour. Allaoui et al. [16] experimentally investigated joint closure behaviour in refractory masonry at ambient temperature. They found that joint closure involves roughness crushing and surface adjustments, which is a heterogeneous, orthotropic, and nonlinear process. Oliveira et al. [6] performed a cyclic joint closure test on alumina-spinel bricks at ambient temperature. They found similar nonlinear joint closing and opening characteristics under normal compressive stress. However, the relation between the gradual closing of joints during cycles was not evaluated. From the literature, it can be observed that most of the research is focused on the joint closure behaviour at ambient temperature. The evaluation of the joint closing and opening behaviour under compressive force cannot be found at high temperatures, where the refractory materials are often used.

Numerical simulations are used to design, predict, or observe the behaviour of masonry structures at various operating temperatures [17–23]. These models can either be a detailed meso-model with bricks and joints, or a macro-model that replaces bricks and joints with a homogenised equivalent material. For both approaches, an accurate representation of a dry joint requires a comprehensive understanding of its behaviour under normal and shear loads at various high temperatures. However, a numerical method to simulate joint behaviour is limited in the field of refractory materials. The Coulomb friction law rules the shear behaviour of the dry joint, and only the friction angle needs to be identified [1,6,15,24]. Oliveira et al. [6] adopted a mathematical model developed by Thanoon et al. [25] for the normal compressive joint behaviour. However, other models of joint closure behaviour that are found in the field of rock mechanics [12,26–29] are not yet evaluated and validated in the research for mortarless refractory masonry. These models are used for the joint deformability under the action of normal compressive forces and the observed behaviour is similar to the behaviour observed for dry joints in mortarless masonry. Validation of such models for dry joint behaviour can be advantageous as these models can be adopted for the framework of numerical simulation.

This study aims to investigate and compare the available analytical models of normal compressive behaviour of dry joints for refractory masonry at various elevated operating temperatures, therefore, contributing to much-needed research in this field. For this purpose, refractory specimens of alumina spinel material with dry joints are tested at ambient and various elevated temperatures, for which no research can be found. The experimental results are then evaluated with different models and efficacy of the models is addressed. Furthermore, one such model is used to validate the finite element models with experiments on mortarless masonry under normal compression at ambient and elevated temperature.

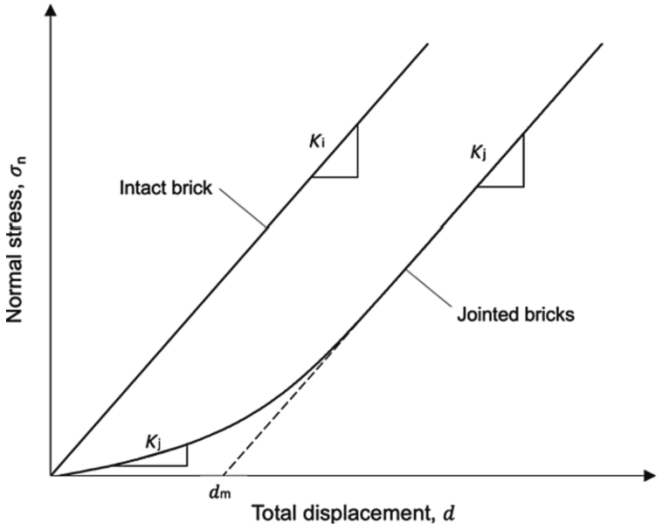

Fig. 3. A schematic of the observed stress-displacement behaviour of intact and jointed bricks specimen under normal compression.

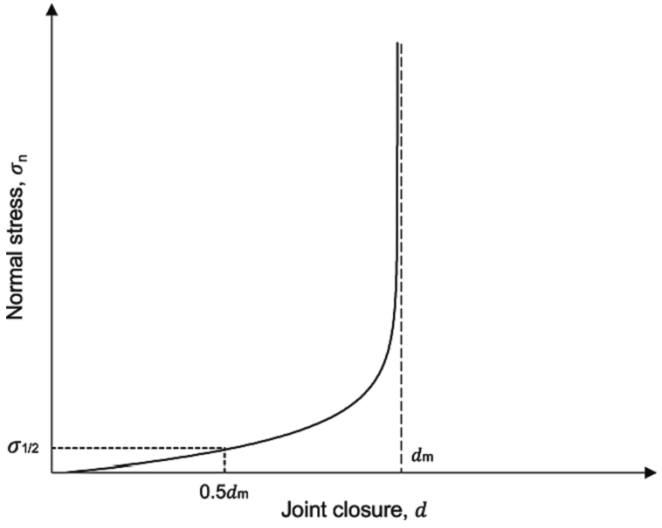

Fig. 4. Normal joint closure behaviour obtained by subtracting behaviour of intact brick specimen from a jointed bricks specimen (adapted from [12]).

2. Review of models for joint closure

Joint closure behaviour under normal compressive loading is described by stress-deformation relations in which the normal stiffness, K_i, and the maximum normal joint closure, d_m, are used as the characteristic parameters (as shown in Fig. 3). For intact brick specimen (i.e., a single brick unit), linear elasticity is assumed, and therefore, the stress, σ_n, as a function of the displacement, d_i, is given in Eq. (1)

$$\sigma_n = K_i d_i \tag{1}$$

where, K_i is the stiffness of the intact brick specimen, assumed to be a constant. As stated earlier, for a brick with dry joint, the relation between the total displacement, d, and the compressive stress σ, normal to the joint, is nonlinear. The stiffness of jointed bricks, K_j, is therefore not a constant but a function of the joint displacement. Experimental and numerical simulation results obtained by several studies observe that the jointed bricks stiffness increases with increasing normal compressive stress, from some lower initial value to that of the intact brick, K_j. That is, the gradient of the $\sigma - d$ curve, K_j, increases, monotonically approaching K_i. Therefore, the jointed bricks experiences two phases: the nonlinear displacement at low pressures and linear elastic behaviour at stresses higher than some stress value related to the mechanical and displacement properties of the joint. The total displacement of jointed bricks, d, is defined in Eq. (2), where d_i is linear elastic displacement of an intact brick and d_n is the joint displacement.

$$d = d_i + d_n \tag{2}$$

The mathematical model proposed by Thanoon et al. [25] that has been used in previous studies for mortarless refractory masonry [6] is shown in Eq. (3). Here, σ_n and d are the normal compressive stress and displacement, respectively. Constants a, b, c are to be determined from data analysis of test results.

$$\sigma_n = ad^b + cd \tag{3}$$

However, for the fracture deformation in rock mechanics (a crack can be assumed as a dry joint in the mortarless masonry), it has been suggested that given the manner in which the normal joint closure tests are conducted, the displacement instead of the stress should be taken to be the dependent variable [12]. In those circumstances, the measured joint properties are best expressed in terms of the normal joint compliance, C_j, rather than the corresponding stiffness. In the simple one-dimensional problem, $C_j = 1/K_j$. However, in the general case, matrix inversion is required, given the tensorial nature of these parameters. Therefore, several mathematical models can be found considering displacement as a dependent variable.

Goodman [26] suggested a hyperbolic relation to describe joint closure under normal compressive stress. Bandis et al. [27] and Barton et al. [29] presented a modification that provided a better fit to experimental data across the whole range of stress and closure values. Malama and Kulatilake [12] further modified the model (Eq. (4)) to express it in terms of final joint displacement, d_m, and stress at the half-joint closure, $\sigma_{1/2}$ (as shown in Fig. 4).

$$d_n = \frac{d_m \sigma_n}{\sigma_n + \sigma_{1/2}} \tag{4}$$

Malama and Kulatikale [12] proposed a generalised exponential model which shows a better fit with a wide range of experimental data. This model (Eq. (5)) is expressed in terms of final joint displacement, d_m, stress at the half-joint closure, $\sigma_{1/2}$, and n is a constant, determined empirically, with $0 < n < 1.0$. This parameter shows variability from one specimen to another.

$$d_n = d_m\left[1 - e^{-(\sigma_n/\sigma_{1/2})^n ln2}\right] \tag{5}$$

These models are expressed considering displacement as a variable providing a more straightforward definition of joint given the relative ease with which the $\sigma_{1/2}$ and d_m could be estimated from laboratory results, when compared to the identification of constants and stiffness values.

Based on Hertzian contact theory, alternative models have also been used to describe the nonlinear joint closure behaviour. These models suggest that the observed nonlinear behaviour could be attributed to the increasing contact areas and the increasing number of contacts as the compressive stress increases. The asperities are assumed to undergo linear elastic displacement [28]. This observation is contrary to the suggestions made by other studies where crushing of the joint surface particles was suggested [6,13,16]. However, this behaviour is not experimentally observed in the literature. Cyclic joint closure experiments are needed to identify the cause behind the observed nonlinear behaviour. This aspect is further discussed in the present paper at the analysis of the experimental data. Applying Hertzian contact theory, Swan [28] proposed a power-law model for crack closure and can be seen in Eq. (6). Here, α and β are constants determined empirically, with $\beta < 1$. However, the observation made by Swan [28] shows that the power-law model provides an excellent fit to experimental data only at low stress levels.

Table 1
Results of the chemical analysis performed on the commercially available alumina-spinel brick used in this experimental campaign.

Chemical	Composition (wt%)
Al_2O_3	94.0
MgO	5.07
Na_2O	0.17
SiO_2	0.16
ZrO_2	0.08
CaO	0.058
Fe_2O_3	0.038
Other oxides	<0.45

$$d_n = \alpha\sigma_n^{\beta} \tag{6}$$

The following sections present a description of the joint closure tests performed at various temperatures for the alumina-spinel refractory material. A comparison of how well the *(i)* generalised exponential, *(ii)* hyperbolic, *(iii)* the power-law, and *(iv)* polynomial models fit of the joint closure data is shown.

3. Joint closure experiments

In this experimental work, alumina-spinel refractory material was used to validate models discussed in previous section. This material is characterised by good chemical and mechanical properties. Scrupulously, it has high refractoriness (the melting temperature of spinel is around 2135 °C) and high resistance to chemical attacks [30,31]. Therefore, this material is frequently used in working linings of steel ladles composed of bricks with dry joints (Fig. 1b-c). The apparent porosity and density of the material are 19 % and 3.13 g/cm^3, respectively [32]. Commercially available bricks were used for this investigation. The chemical composition of this material is presented in Table 1. The composition is found to be similar to the recommended values for this material [6,31]. The geometry of the brick is a trapezoidal prism with 140–160 × 140 × 100 mm^3, as shown in Fig. 1a. These bricks are produced from natural raw materials. The bricks are moulded at a hydraulic press and fired at high temperatures.

These bricks are subjected to transient thermal loading and have a thermal gradient while in operation. To create a similar condition in laboratory is complex and often requires large scale experiments. Therefore, tests are performed at specific temperature levels to evaluate mechanical properties of the materials, such as compressive strength, tensile strength, creep, etc [5,32] and use it in numerical simulation to evaluate the global response. Similarly, the joint closing behaviour in this work is observed by applying a normal compressive force to the specimen with joints at different temperatures. In this method, the compressibility of the joint is determined by the force–displacement behaviour of the specimens. Cylindrical samples are tested for this purpose. The specimens with the joint consist of two stacked pieces with a diameter of 50 mm. The height of each piece is 25 mm. The samples were carefully drilled from the bricks using a diamond core driller. Cylindrical specimens of this size are used due to the size limitations of the furnace used to perform joint closure experiments at high temperatures. This approach was also adopted by Andreev et al. [13] to perform joint closure experiments of magnesia carbon and magnesia chromite brick specimen. The prepared specimens were carefully dried by placing them in a drying oven operating at 110 °C for 24 h and then cooled to room temperature and stored in a dry place till the test.

As already described, the nonlinear behaviour of the dry joint is primarily dependent on the composition of the joint surfaces (i.e., surface roughness, contact area distribution and parallelity of the bonding surfaces) and material type. Therefore, the definition of the bounding surfaces is a variable. To obtain the joint closure behaviour of the alumina-spinel brick at various temperature ranges and to compare its mechanical performance, the definition of the bounding surfaces should be similar for all the specimens. However, the roughness and parallelity present in a surface with the original face of the brick (i.e., the exterior surfaces) varies among the specimens. Therefore, the bounding surfaces of the joint were carefully cut and plan-paralleled to achieve a similar range of surface roughness and parallelity between various specimens. The surface roughness achieved with this process provided a similar

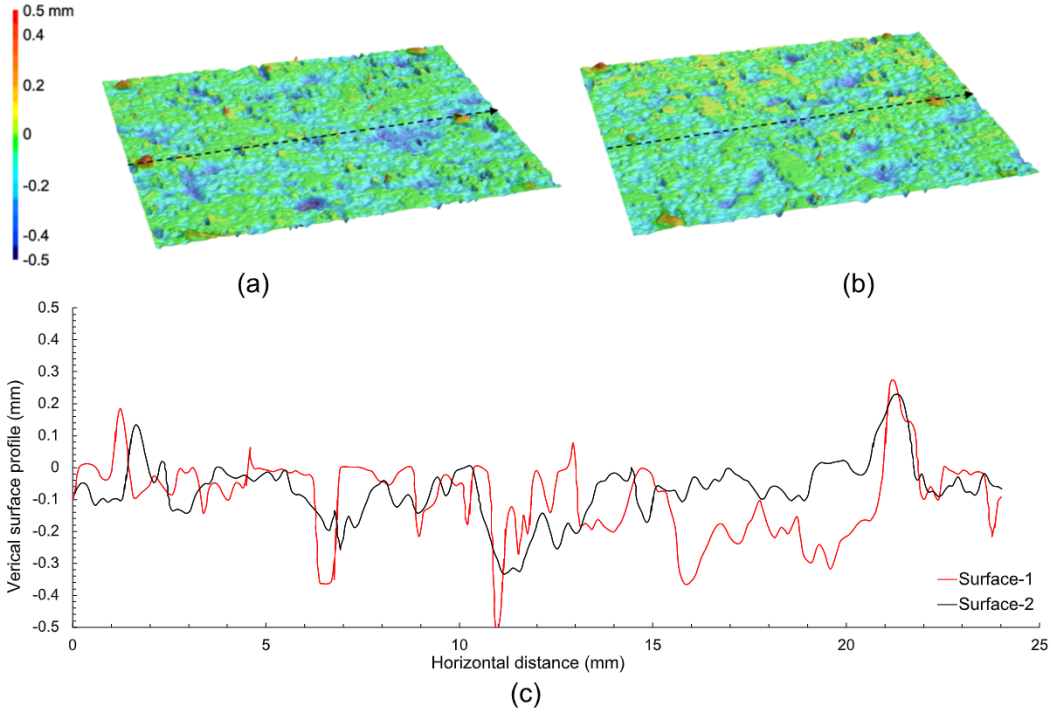

Fig. 5. Definition of the surfaces for the joint closure experiments: a) example of 3D map on surface 1; b) 3D map on surface 2; c) plot of the vertical surface profile (black dashed line from 3D surface maps).

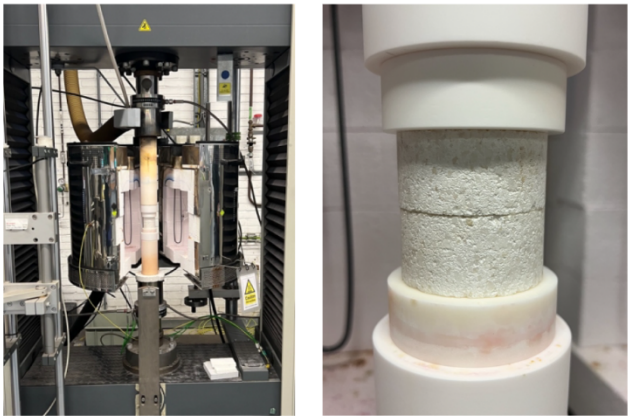

Fig. 6. Joint closure test at high temperature - Experimental setup: a) overview and b) detail of specimen.

definition of the surfaces across all the samples. Configuration of the prepared surfaces was evaluated by performing a 3D measurement macroscope using the Keyence VR-3100 device. Such scans provided confirmation of the prepared surfaces (Fig. 5). Examples of 3D measurement scans taken from the central part of the specimen are shown in Fig. 5a-b for two prepared surfaces. From the plot of vertical surface profile plot from the centre of the measured area (Fig. 5c), it can be observed that for both the surfaces, the range of variation is similar, with an average of 0.91 mm and 0.80 mm for specimen 1 and 2 respectively. At some locations in the specimens, a more prominent difference could be observed due to the cutting process. However, considering the profiles it was assumed a similar range of joint thickness for all the specimens, so that the relation between joint closure behaviour at various temperatures can be established.

A normal compressive force is applied on the prepared cylindrical specimens by using a universal mechanical test frame Zwick/ Roell Z250 with a maximum capacity of 250 kN (Fig. 6a). The compressive force is applied with a constant displacement rate of 0.005 mm/s for all tests. This displacement rate was selected within the range observed in the literature for compressive tests on refractory materials [6,13]. The prescribed stress levels were observed through the load cells in the testing machine. Through the testing software, once the desired load is achieved the displacement increment is stopped and the unloading starts at the same displacement rate. Once the specified minimum load level is achieved (0.15 MPa) the unloading stage is over. For the experiments at high temperatures, the specimens are heated up at a rate of 5 °C/min. Samples are conditioned at the desired test temperatures for 90 min to ensure uniform distribution of temperature within the specimen (dwell time). During the test, the temperature was only monitored in the furnace, however, previous tests on the same material showed homogenised temperature throughout the specimen, even for dwell times of 60 min and specimens of larger dimensions [6]. The furnace accuracy is ± 0.5 % of the desired test temperature. A 0.3 kN (≈ 0.15 MPa) compressive force was applied for the heat up and conditioning duration to keep the specimen aligned during the thermal expansion. The used rates of heat-up and displacement represent average service conditions and are standard for high temperature tests of refractories. Sample displacement during the test is measured by the machine cross head travel, corrected for the machine's internal displacements. The displacement results are validated by a finger extensometer. The resolution of the former and latter systems are ± 0.5 % of the displacement and ± 0.1 μm, respectively. The tests were performed at ambient temperature, 600 °C, 800 °C, 1000 °C, and 1200 °C. The applied maximum compressive stress is 18 MPa for all the performed tests. It should be noted that only one specimen per each temperature range was tested, as the primary objective is to evaluate the performance of the analytical models described in section 2.

4. Analysis of normal joint closure data

Alumina-spinel bricks belong to the disordered heterogeneous material class. Their microstructure and mechanical behaviour resemble to those of concrete and stones. Under compression, the bricks show an initial linear-elastic response followed by micro-crack formation. At lower temperatures, their behaviour is brittle, while at high temperatures, it becomes ductile. The material stiffness and strength are strongly temperature dependant. At higher temperatures, visco-plasticity dominates the material response to the compressive loads [33].

Normal compressive tests were carried out first on single brick specimens to evaluate the linear elastic behaviour. For this purpose, three samples were tested till 18 MPa by applying loading cycles at 3, 6, 9, 12, 15, and 18 MPa. The test was stopped at 18 MPa as it corresponds to 50 % of the compressive strength of the material [5] to avoid inelastic deformation. These tests were performed according to the guidelines from EN 993–5:2000 "Methods of test for dense shaped refractory products, Part 5: Determination of cold crushing strength" [34]. Fig. 7a shows the stress–strain behaviour of the alumina-spinel specimens at ambient temperature. The figure indicates a linear-elastic response.

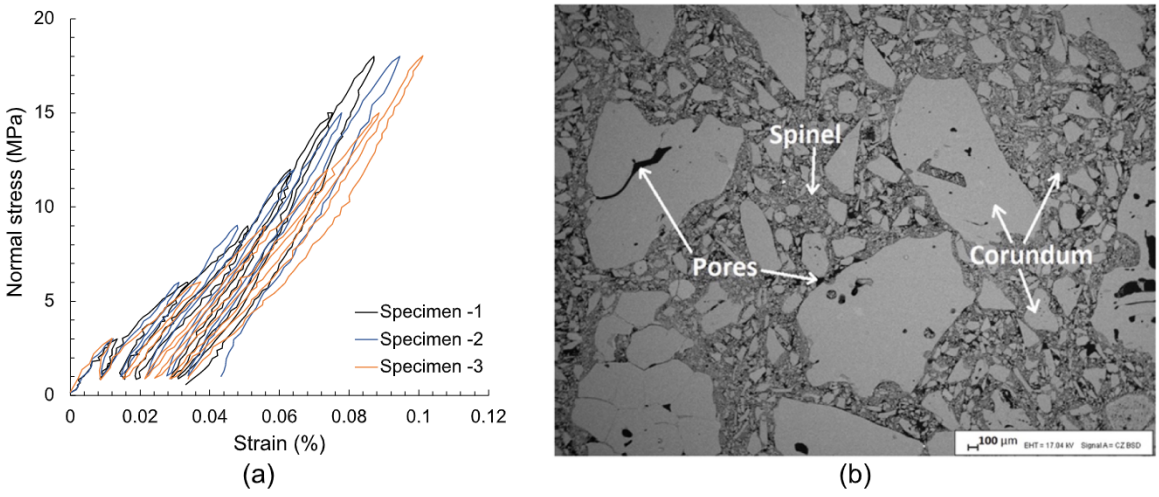

Fig. 7. Normal compressive behaviour of alumina-spinel material at ambient temperature: a) stress–strain diagram presenting experimental results of normal compressive tests performed on single brick specimens; b) example of the microstructure of the material showing grains (corundum), matrix (spinel) and pores [32].

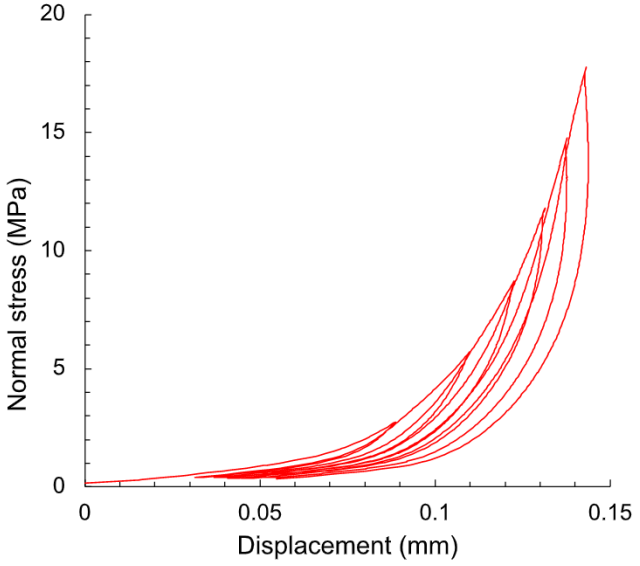

Fig. 8. Experimental stress-displacement result of joint closure test at ambient temperature.

Table 2
Parameter values used in different models for alumina-spinel specimens tested at ambient temperature.

Model	Parameters	Values
Exponential model	d_m(mm)	0.119
	$\sigma_{1/2}$(MPa)	1.20
	n(-)	0.80
Hyperbolic model	d_m(mm)	0.130
	$\sigma_{1/2}$(MPa)	1.20
Power-law model	α(-)	0.068
	β(-)	0.22
Thanoon model	a(-)	4.45×10^8
	b(-)	7.81
	c(-)	15

During initial loading, the calculated Young's modulus ranges from 19 to 21 GPa. However, strain hardening can be observed in the applied pre-peak cycles. This behaviour is due to the microstructure of the material (Fig. 7b), which is composed of alumina grains (corundum), matrix (spinel) and pores [32]. As the applied compressive stress increases, the pores present in the microstructure are closed. Therefore, such material behaviour should be considered while evaluating the joint closing and opening behaviour.

4.1. Joint closure tests at ambient temperature

Fig. 8 presents the stress-displacement result obtained from the joint closure test performed on a specimen at ambient temperature. The figure shows that a nonlinear behaviour dominates the behaviour at lower stress levels (up to 5 MPa) due to increasing surface contact as the smaller surface asperities crushes. At higher stress levels, the joint specimens were observed to be following the linear-elastic response of a single brick. This outcome confirms the typical joint closing behaviour described in the literature [6,13,16]. It can also be observed that for the loading cycles performed at various stress levels, the observed linear-elastic behaviour of specimens increases, primarily due to strain hardening. However, nonlinear behaviour induced by the joint is similar for all the loading cycles. A plastic deformation of 0.03 mm can be observed after the first loading cycle. For the successive loading cycles, an average deformation of 0.004 mm was obtained. These values are calculated by subtracting the displacement obtained at the end of each loading cycle with the value observed during previous loading cycle.

To evaluate the joint closing behaviour with mathematical models presented in section 2, inverse identification of the joint parameters was performed to achieve the best possible fit. For this purpose, the loading and unloading behaviour up to 18 MPa is considered for better visualisation. This characterisation is sufficient as the observed behaviour is linear from 10 MPa. The values used for different models are shown in Table 2. The joint displacement behaviour obtained by these models are shown in Fig. 9a, and the joint closure behaviour is shown in Fig. 9b. The joint displacement is evaluated by calculating the joint closure profile from the different models and adding the linear-elastic behaviour observed in the specimen at high stress levels. For the specimen tested at the ambient temperature, the observed Young's modulus is 21 GPa, which is similar to the average value from the intact reference specimen (Fig. 7a). From Fig. 9a, it can be observed that all the models can represent the nonlinear behaviour at the lower level of stresses, being in good agreement with the experimental observation.

However, for the global behaviour, only the Exponential and Hyperbolic models are observed to be in good agreement. The evaluated value of joint closure is 0.12 mm and 0.13 mm for the exponential and hyperbolic models, respectively. The difference between these values is about 8 %. The stress value at half joint-closure ($\sigma_{1/2}$) is 1.2 MPa for both models. As stated earlier, the exponential and hyperbolic models are

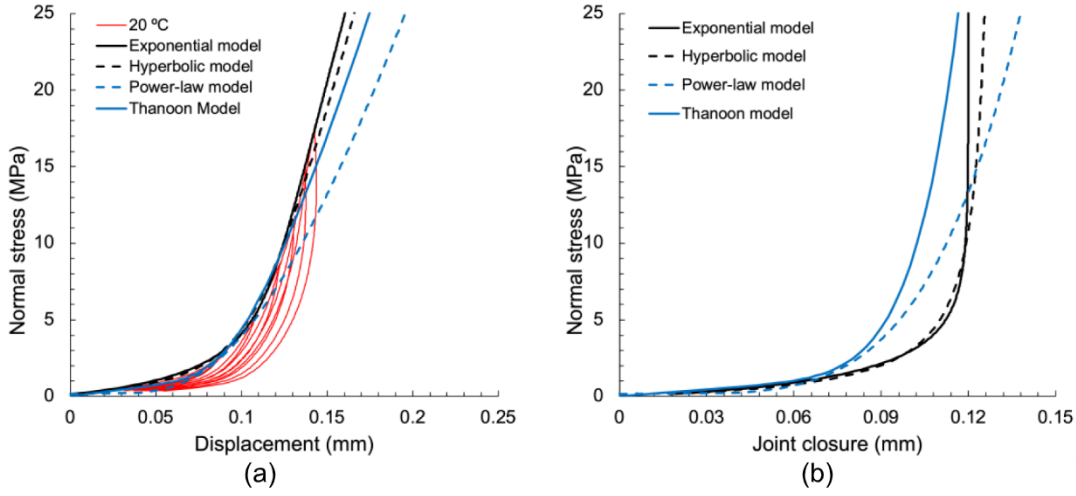

Fig. 9. Result of joint closure test performed at ambient temperature: a) experimental result and model fits using parameters values given in Table 2; b) joint closure behaviour obtained by various models.

Table 3
Parameter values used in different models for alumina-spinel specimens tested at various elevated temperatures.

Model	Parameters	Values			
		Temperature (°C)			
		600	800	1000	1200
Exponential model	d_m(mm)	0.065	0.056	0.048	0.041
	$\sigma_{1/2}$(MPa)	1.0	0.9	0.8	0.6
	n(-)	0.80	0.75	0.80	0.80
Hyperbolic model	d_m(mm)	0.080	0.058	0.053	0.045
	$\sigma_{1/2}$(MPa)	1.0	0.9	0.8	0.6
Power-law model	α(-)	0.040	0.024	0.025	0.080
	β(-)	0.250	0.260	0.300	0.112
Thanoon model	a(-)	1.89 × 10^6	7.23 × 10^6	2.99 × 10^6	4.25 × 10^5
	b(-)	4.55	4.28	4.20	2.90
	c(-)	25	25	35	50

advantageous in obtaining the joint closure behaviour. They rely on the physical parameters (joint thickness and stress at half joint-closure) that can be obtained from the experimental data through inverse analysis. In the case of the Power-law and Thanoon model, the parameters' values need to be obtained empirically, without a physical significance. From Fig. 9b, it can be noticed that the joint stiffness given by the exponential and hyperbolic models are higher, which suggests the complete closure of the joint. In contrast, the other two models imply an open joint even at higher stress levels.

4.2. Joint closure tests at elevated temperatures

The joint closure test results obtained at elevated temperatures are presented in this section. A similar procedure is adopted as in the previous section to evaluate the joint closing behaviour. The derived values of the Young's modulus from the observed linear response at high stress levels (between 10 and 15 MPa) are 13.5, 9.75, 7.5 and 4.35 GPa at 600 °C, 800 °C, 1000 °C, and 1200 °C, respectively. Table 3 presents the values of the parameters calculated to obtain the best possible fit with the different models. The joint displacement behaviour is obtained by adding the linear elastic response of the material in the joint closure models at various temperatures.

Fig. 10 presents the experimental results and response obtained with different models at different elevated temperatures. From the experimental results, it is possible to observe the reduction in the material stiffness at high-stress levels with the increase in the temperature. This reduction is due to the gradual degradation of the material properties with increased applied temperatures. Fig. 11 shows the degradation indicated by the rise in the plastic displacement between different loading cycles with respect to the different temperatures. These values are calculated by subtracting the displacement obtained at the end of each loading cycle with the value observed during previous loading cycle (i.e., subtracting displacement obtained after load cycle 2 with load cycle 1). From Fig. 11, a significant plastic deformation can be observed after the 1st load cycle till 3 MPa for all temperatures. For subsequent load cycles at 600 °C, 800 °C and 1000 °C, an average plastic deformation of 0.005, 0.007 and 0.01 mm can be observed. However, for

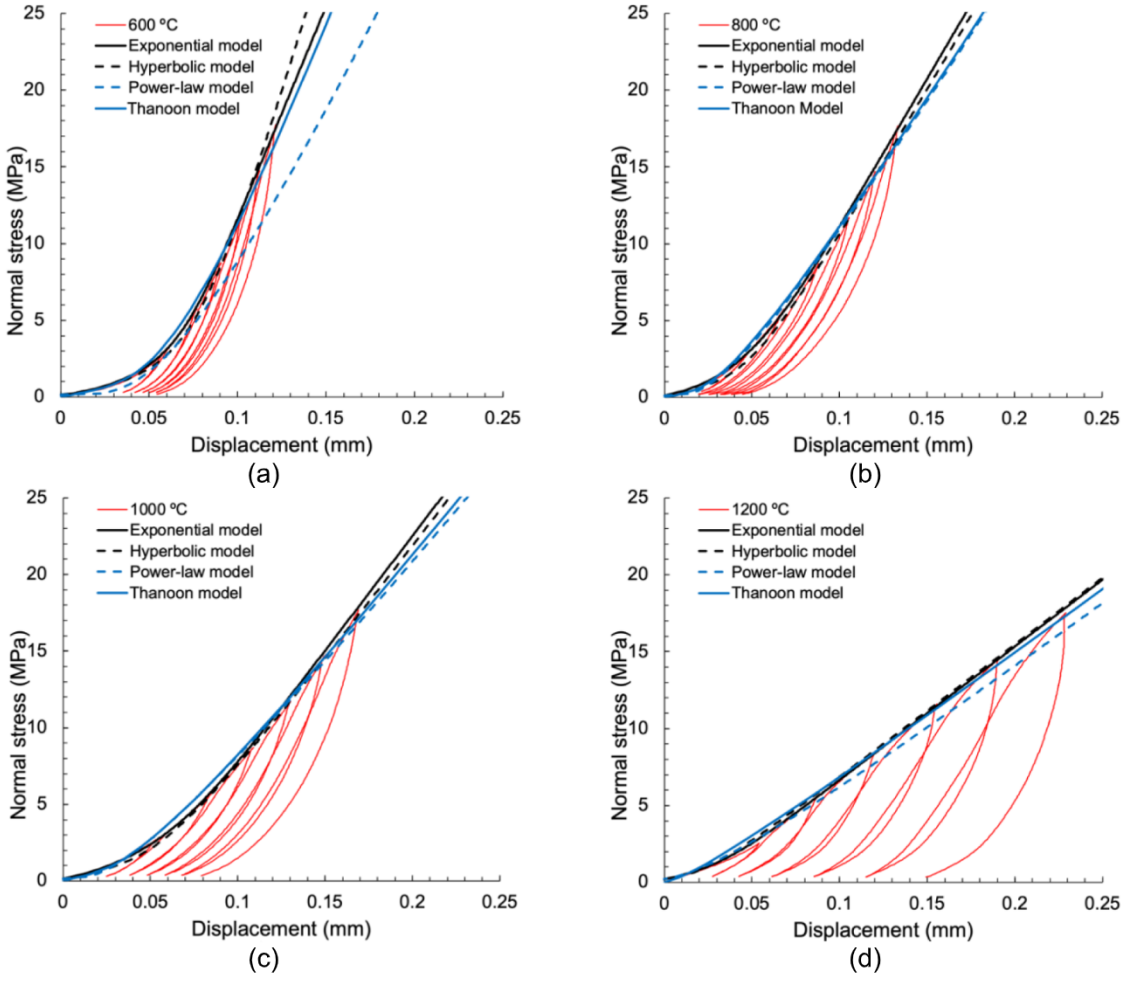

Fig. 10. Experimental results and model fits using parameters values given in Table 3 for joint closure tests performed at elevated temperatures: a) 600 °C; b) 800 °C; c) 1000 °C; d) 1200 °C.

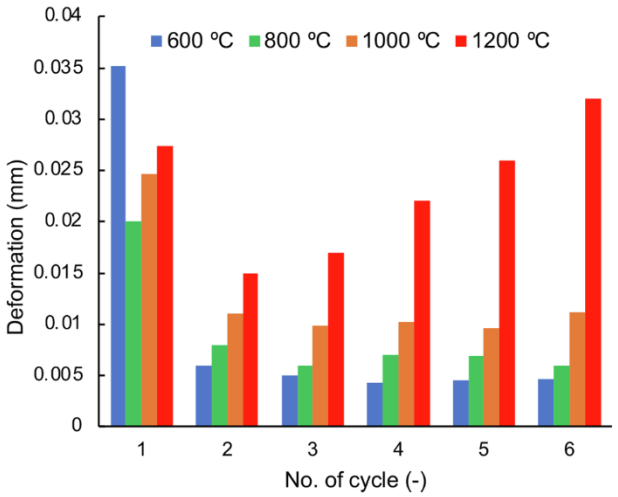

Fig. 11. Plastic deformation at different temperature, at the end of each loading cycle.

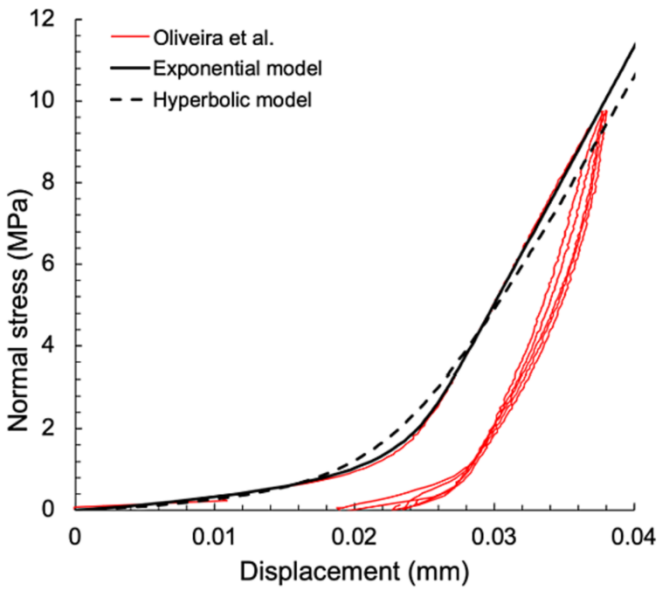

Fig. 12. Experimental result obtained by Oliveira et al. [6] and model fits.

the 1200 °C, the deformation increases from 0.015 to 0.032 mm from load cycle 2 to 6. This increase can be caused by the strain hardening. However, it can be observed that for all temperatures, the joint closing behaviour stays similar after the first load cycle at 3 MPa (Fig. 10). This behaviour is identical to the observed behaviour at ambient temperature. This suggests that at 3 MPa, the smaller asperities (i.e. the surface roughness) are crushed. Only the larger asperities remain in the joint surface, which seems to follow the linear elastic deformation. This observation is similar to the prediction made by Malama and Kulatilake [12]. They suggest a mixed response arising from the crushing of the smaller asperities and the elastic behaviour of larger asperities in the joint surfaces.

The model fits achieved with the inverse identification of the parameters (Table 3), provide a good agreement with the initial nonlinear response of the joint closure (Fig. 10). However, the linear elastic response obtained by the power-law model and model proposed by Thanoon at the high stress level does not show a good agreement with experimental results at 600 °C (Fig. 10a). This observation is similar to the behaviour obtained with this model at ambient temperature. It is interesting to observe that all models present a good fit with the experimental data at 800 °C, 1000 °C, and 1200 °C (Fig. 10b-d). These figures show that the power-law and Thanoon models better represent the joint behaviour for materials with lower stiffness at higher temperatures. Although these models offer a relatively better fit at these temperatures, the parameters' values need to be identified empirically, which is harder to evaluate from the experimental data. These parameters are not related to the properties of the joint and thus cannot be quantified with it.

The exponential and hyperbolic models seem to better describe the joint closure behaviour across all the range of tested temperatures. Moreover, these models use parameters related to the joints' properties (i.e., joint thickness and stress at half-joint closure). This relation provides an advantage over other models as the parameters for these models can be easily identified and quantified from the experimental data, with the inverse identification. However, one additional parameter (n) must be determined for the exponential model, which seems more complicated to quantify with the joints' properties. This parameter may be a function of material type, roughness and loading history, as suggested in [12]. Therefore, the hyperbolic model, first proposed by Goodman [26], seems to offer an advantage over other models discussed in this work. The parameters required for this model can be easily obtained from the experimental results. The model seems to better fit the joint closure behaviour at all the different tested temperatures for the alumina-spinel specimens. However, the values for the joint closure identified by this model are higher than those determined experimentally (by extending the linear elastic part observed at higher compressive force to zero, as presented in Fig. 3). The joint thickness values obtained by the exponential model seem to offer a good agreement with the values observed experimentally. This difference is due to the formulation of the models. The hyperbolic model assumes a very high normal stress requirement for the joint closure, which is contrary to the results obtained in this series of experiments.

To evaluate the response of these models for full size bricks with the same material (larger contact surface), the experimental result obtained by Oliveira et al. [6] is used. In the dry joint of bricks, apart from surface roughness, gaps are also present due to the unevenness of the bounding surfaces. The obtained response of these models and the experimental result is shown in Fig. 12. The observed value of the joint thickness is 0.022 mm, and the stress at half joint closure is 0.5 MPa. From the figure, it can be observed that the exponential model represents identical experimental behaviour for a larger surface. In contrast, the hyperbolic model has difficulties in reproducing the transition from the nonlinear closing to linear elastic regimes. The ability of exponential model to represent the transition is due to parameter n, which grants an additional degree of freedom.

Therefore, considering all aspects of different models, the exponential model seems to represent the joint closure behaviour better across all ranges of tested temperatures and different sizes of specimens. This model can also represent the joint closing behaviour of bricks. The ability of this model to adapt to larger scales (i.e., mortarless masonry) is described and validated with a finite element analysis in the numerical modelling section. Fig. 13a shows the joint closure behaviour obtained by the exponential model for all the test series discussed earlier. It is clear from the figure that the joint thickness reduces with an increase in the applied temperature. This behaviour was expected due to the material's thermal expansion and reduced stiffness, which decrease the gap in the joint. As the applied temperature increases, the material stiffness will decrease, and material will expand. Due to this action, the surface roughness will decrease, resulting in smoother joint. Strong influence of the temperature on joint closure was also documented by Andreev et al [13]. They attributed thermal expansion of the material as the most probable cause of the joint thickness reduction. Fig. 13b shows the reduction in the observed joint thickness and dilation of the alumina-spinel material (dilation measurements taken from Kaczmarek [35]). This data indicates that there might be a linear relationship between the reduction in the joint thickness and the dilation of the material.

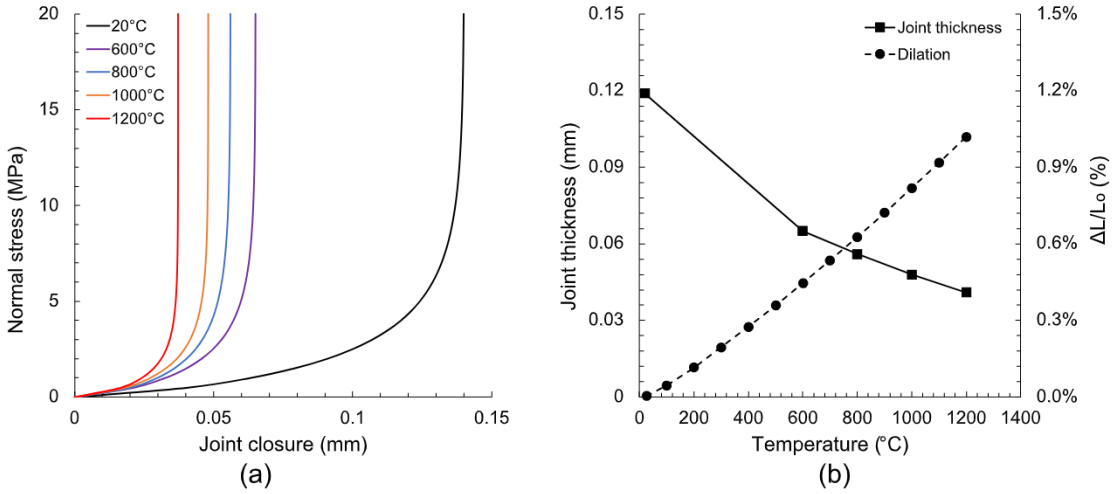

Fig. 13. Joint closure behaviour: a) model fits obtained by the exponential model at various tested temperatures for alumina-spinel specimen; b) chart showing a reduction in joint thickness of the tested specimen with an increase in temperature along with dilation of material [35].

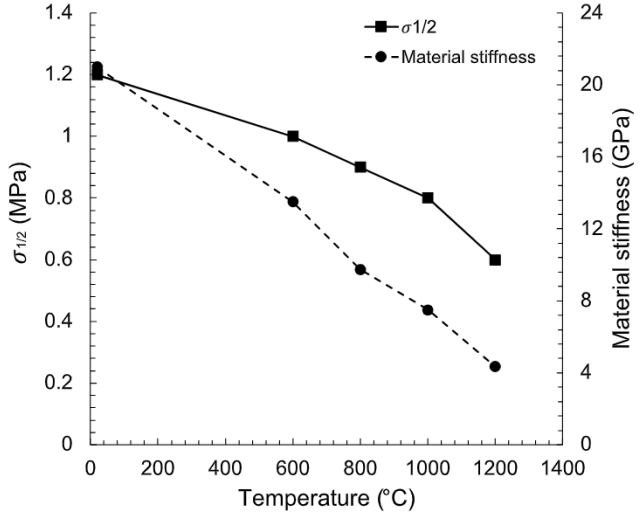

Fig. 14. Stress at half joint closure ($\sigma_{1/2}$) and material stiffness of the tested specimen at different temperatures.

Fig. 14 presents the evolution of the stress at half joint closure ($\sigma_{1/2}$) and material stiffness with an increase in applied temperature. It is evident from the figure that the initial stiffness of the joint decreases as the temperature increases. This reduction is due to the degradation of the material properties at higher temperatures as it allows surface asperities to undergo large displacement under relatively minor compressive stress. It can be observed that the relation of these parameters is approximately linear with respect to the temperature. Moreover, it can be noticed that there may be a linear relationship between the reduction in $\sigma_{1/2}$ and material stiffness. Moreover, behaviour of such refractory material under compression is scattered at ambient temperature (as shown in Fig. 7a) and possibly even more at elevated temperatures. Therefore, the experimental results presented should be used as a trend, where the expected change in joint closing behaviour can be understood. To establish a more comprehensive relation with material properties and geometric parameters, additional experiments are required at each temperature level.

The unloading and reloading behaviour of a dry joint is complex to analyse. During the unloading step, the material itself exhibits a nonlinear behaviour due to strain hardening. Therefore, to evaluate only the dry joint behaviour for the unloading and reloading, the joint closure is assessed for the last loading cycle in all the specimens (i.e., from 0.15 MPa to directly up to 18 MPa). Although not wholly evaluating the actual unloading behaviour of the joint, this approach was deemed satisfactory. Table 4 shows the values of the parameters identified for the reloading behaviour through the exponential model for all the samples presented previously. Fig. 15 shows the model fits along with the experimental results for the last loading cycle. From the figure, it can be observed that the exponential model fits well with the reloading of

Table 4
Parameter values used in the exponential model for specimens subjected to reloading from 0.15 MPa to 18 MPa at various temperatures.

Temperature (°C)	d_m (mm)	$\sigma_{1/2}$ (MPa)	n (-)
20	0.071	1.5	0.8
600	0.036	1.2	0.8
800	0.040	1.2	0.9
1000	0.032	1.1	0.8
1200	0.026	0.9	0.8

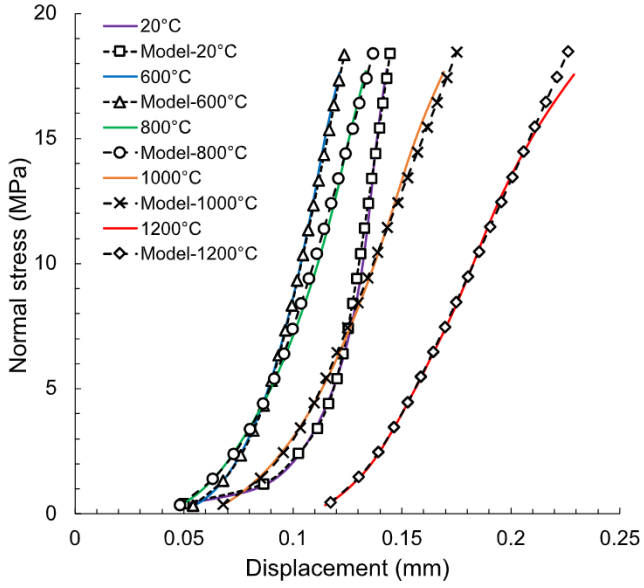

Fig. 15. Experimental results and model fits using parameters values given in Table 4 for joint reloading at various temperatures.

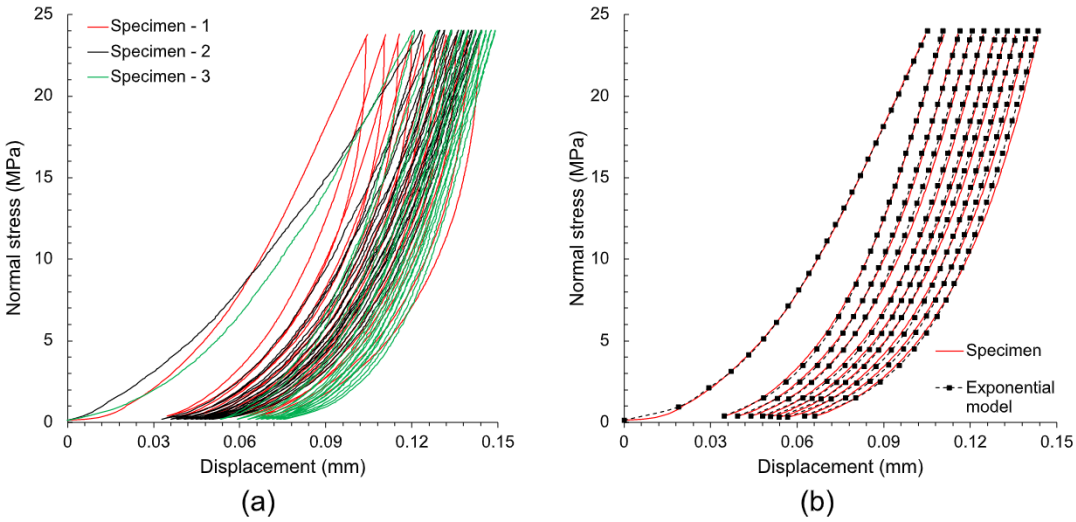

Fig. 16. Stress-displacement diagram presenting experimental results of cyclic joint closure test performed on alumina-spinel specimens at ambient temperature: a) experimental result; b) exponential model fit at all loading cycles of specimen 1.

Table 5
Parameter values used in the exponential model for specimens subjected to cyclic loading at ambient temperature.

Cycles	d_m(mm)	$\sigma_{1/2}$(MPa)	n(-)
1	0.055	1.2	0.75
2	0.037	1.5	0.75
3	0.037	1.5	0.75
4	0.037	1.5	0.75
5	0.037	1.5	0.75
6	0.037	1.8	0.75
7	0.037	1.8	0.75
8	0.037	1.8	0.75
9	0.037	1.8	0.75
10	0.037	2.0	0.75

the samples at various temperatures. It can be noticed that, at a higher temperature, after the joint is assumed closed, the linear-elastic behaviour does not fit well with the experimental data. This difference is due to the nonlinear reloading behaviour of the material, as stated earlier.

Nevertheless, the identification of the dry joint properties, shown in Table 4, suggests a decrease in the joint thickness from the initial value due to the crushing of the surface roughness. Interestingly, the difference in thickness is 0.048 mm (40 %) at the ambient temperature, and it reduces to 0.015 mm (36 %) at 1200 °C. This reduction in joint reclosing with increased temperature is due to reduced material stiffness and plasticity at a higher temperature. Moreover, it can be observed that the stress required for the half-joint closing increases at higher temperatures. This increase can be attributed to the reduced joint thickness, which reduces the surface asperities and increases the contact area between the surfaces.

4.3. Cyclic joint behaviour

Cyclic joint closing tests were carried out on two cylindrical specimens to evaluate the effect of cyclic loading application. These tests were performed only at ambient temperatures. As discussed in previous sections, a similar experimental procedure is followed for these tests. The specimens were subjected to 10 cycles of loading up to 24 MPa. Experimental results obtained from these tests are presented in Fig. 16a. It can be observed that the behaviour is similar to the other specimens tested at ambient temperature, in which a significant change in stiffness can be observed due to strain hardening from the initial load cycle to the second loading cycle. However, it can be noticed that the stiffness does not change substantially for the subsequent load cycles. Moreover, after ten cycles of loading, the effect of a dry joint can be observed, which suggests that the surface asperities are still present.

Inverse identification of the parameters is similarly made for each loading cycle as in the previous section to quantify these observations. Table 5 presents the identified values of the parameters for the exponential model. For better visualisation, experimental data and model fits for the loading at each cycle are shown in Fig. 16b for one specimen only. From Fig. 16b and Table 5, it can be observed that the value of joint thickness decreases from the initial cycle to the second load cycle due to the crushing of the surface asperities. However, it can be observed that the value of joint thickness does not change for the subsequent loadings. This suggests that the shift observed in the experiments is primarily due to material behaviour and not the dry joint. The stress at half-joint closing stays identical for the initial cycles for the loading but increases after the 5th cycle of loading. This change can be caused by the degradation of the particles on the surface due to repetitive loadings. The values of parameters shown in Table 4 and Table 5 indicate that the value of n does not change in the evaluation of different loading cycles. This observation suggests that n can be related to the distribution of asperities in the bounding surfaces of a joint.

Furthermore, no change in the joint thickness after the second loading cycle shows that only the smaller asperities are crushed, and larger particles on the surface undergo elastic deformation. Before and after the experiment, 3D measurements of the surfaces were obtained for the specimen to assess the surface profile. It should be noted that the specimen used for this test is with low surface roughness. Fig. 17a and b show the surface definition of the top and bottom surface of the joint. The figures show that the global distribution of the asperities does not change much even after the ten cycles of normal compressive loading. Only minor changes can be observed in terms of the removal of protruding surface particles. The vertical surface profiles shown in Fig. 17c confirm the observation. These figures and the experimental results indicate that only minor, protruding surface particles get crushed during the initial load application. The global surface exhibits elastic behaviour for the subsequent loading. However, this is assumed true only for the material tested in this study and the stress level applied in experiments.

5. Numerical modelling

In the previous sections, the efficacy of the exponential model is shown for the dry joint with a small surface area. To evaluate its performance at a larger scale (i.e., mortarless masonry), numerical

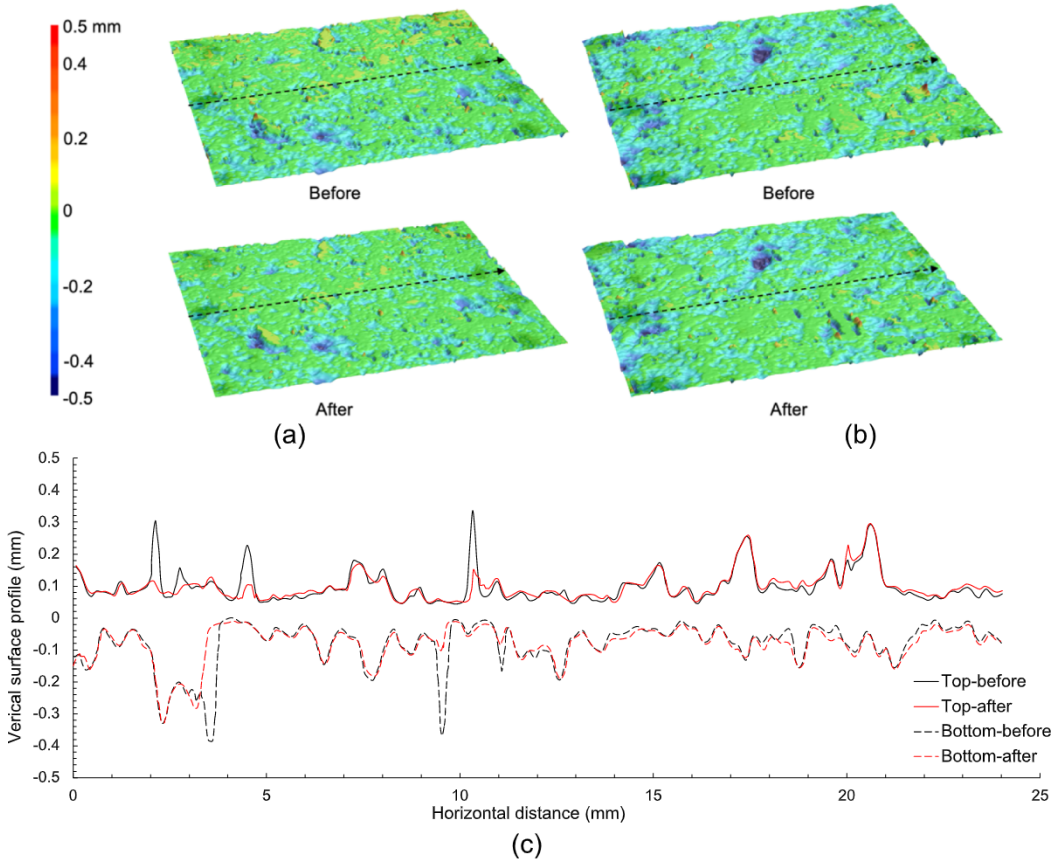

Fig. 17. Change in the surface definition before and after the cyclic load experiment at ambient temperature: a) top 3D surface map of the specimen 1; b) bottom 3D surface map of the specimen 1; c) vertical surface profile (black dashed line from 3D surface maps) taken before and after the experiment.

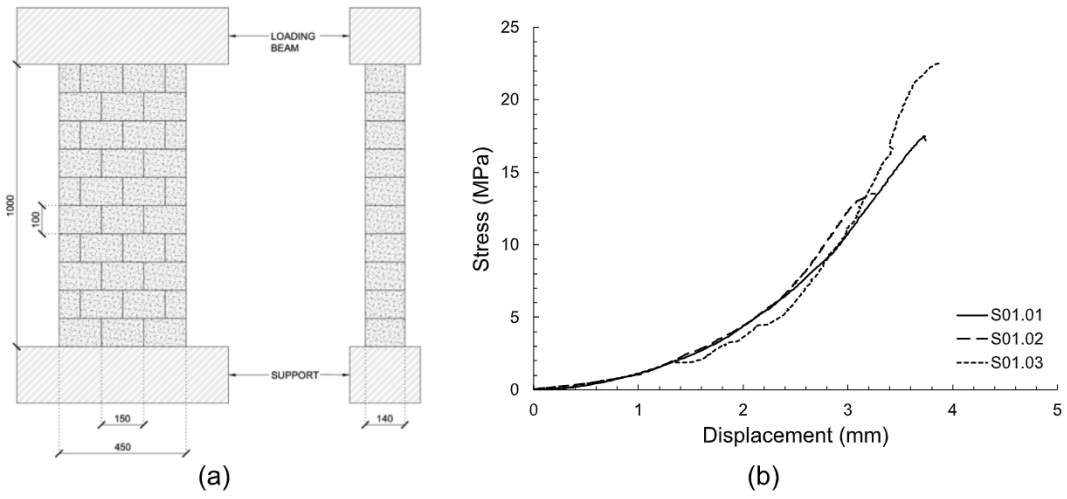

Fig. 18. Uniaxial compression experiments on mortarless masonry: a) graphical representation of the experimental setup; b) stress-displacement results obtained from experiments (adapted from Oliveira et al. [5]).

simulation using finite element modelling (FEM) is discussed in this section. For this purpose, numerical simulations are validated with experimental results at ambient temperature and at 1200 °C in following sections.

5.1. Numerical modelling at ambient temperature

For numerical simulation at ambient temperature, an experiment previously performed by Oliveira et al. [5] on mortarless masonry with alumina-spinel bricks is considered. This test was performed up to the failure of the masonry wall. The geometry of this test is shown in Fig. 18a. The results obtained from these experiments (three equal specimens) are presented in Fig. 18b. It shows a nonlinear response during the initial loading due to the closing of the dry joints. Once the joints are closed, a linear response up to the failure of the wall is obtained.

The meso-modelling approach is selected for numerical simulation, where the units and joints are modelled separately [18]. Finite element

Table 6
Parameters of the alumina-spinel brick for the CDP model.

Young's modulus (E)	21000 MPa
Density	3130 kg/m^3
Dilatation angle (ψ)	20 °C
Eccentricity (ϵ)	0.10
f_{b0}/f_{c0}	1.16
K_c	0.667
Viscosity parameter	0.02
f_c [MPa]	27.4
f_t [MPa]	4.3
G_f [J/m^2]	111.7

analysis is carried out in Abaqus 2019 [36], using available constitutive models for the material and interfaces (i.e., dry joints). The Concrete Damage Plasticity (CDP) model was used for the brick units. This model allows failure under compressive crushing and tensile cracking. The CDP model is a modification of the Drucker-Prager model [37,38], where the shape of the failure surface in the deviatoric plane does not need to be a circle, and it is defined by the parameter K_c. This parameter can be defined as a ratio of the distances between the hydrostatic axis and the compression meridian, and the tension meridian in the deviatoric plane. This parameter was taken as 0.667, as recommended in [36].

Similarly, the dilation angle (ψ) was taken as 20°, the eccentricity (ε) defines the rate at which the flow potential approaches the asymptote (tends to a straight line as the eccentricity tends to zero) and was taken as 0.10, the ratio of the initial equibiaxial compressive yield stress (f_{b0}) to initial uniaxial compressive stress (f_{c0}) as 1.16 and the viscosity parameter as 0.02, used to improve the convergence rate in the softening regime. Table 6 presents the complete mechanical properties adopted in the numerical model. The Young's modulus (E) and compressive strength (f_c) of the material are taken from the tests performed by Oliveira et al. [6]. The tensile strength (f_t) and fracture energy (G_f) were obtained by wedge split test performed by Kaczmarek et al. [39] for alumina-spinel material.

In mortarless masonry, the joint thickness is not uniform for all the joints present, due to surface unevenness and tolerances in dimensions

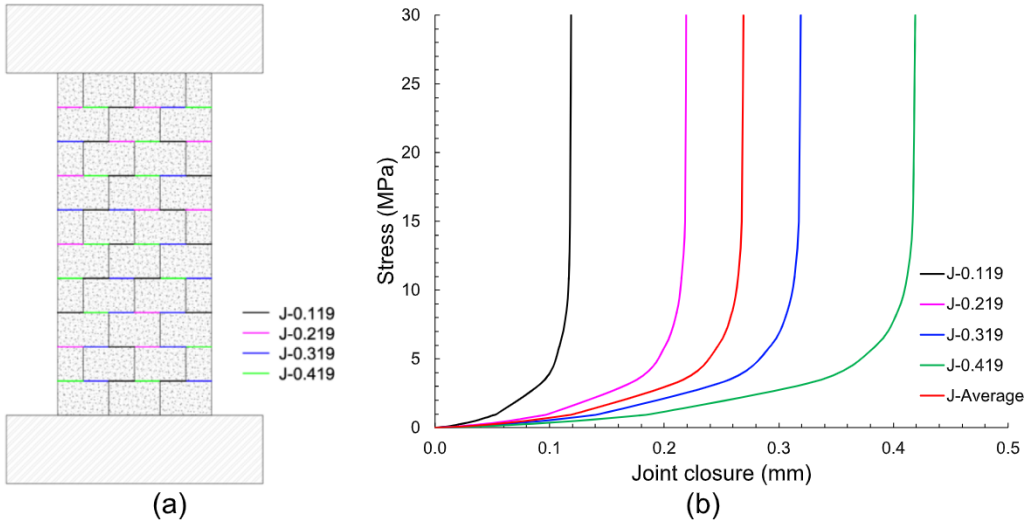

Fig. 19. Distribution of joint thickness for bed joints: a) graphical representation of distribution at bed joints; b) joint closure relation for different thicknesses.

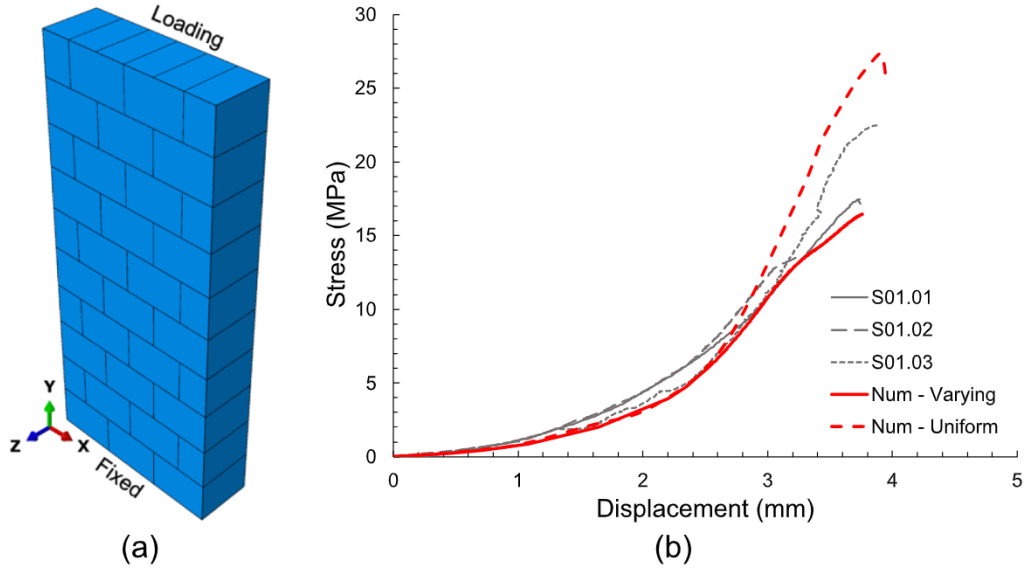

Fig. 20. Numerical analysis: a) meso-model for the uniaxial compressive test simulation presenting individual brick units; b) stress-displacement profile from experiments and numerical simulations. Num - Varying indicates a model with random varying joint thicknesses. Num - Uniform shows the model with uniform average joint thickness.

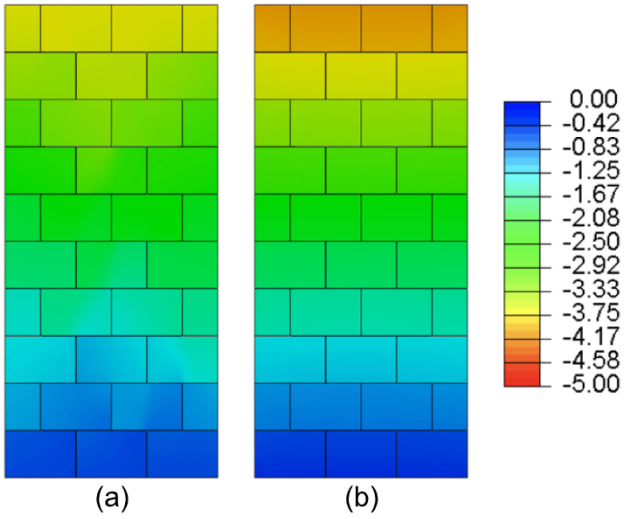

Fig. 21. Vertical displacement (in mm) due to applied peak compressive force: a) model with varying joint thicknesses; b) model with uniform joint thickness.

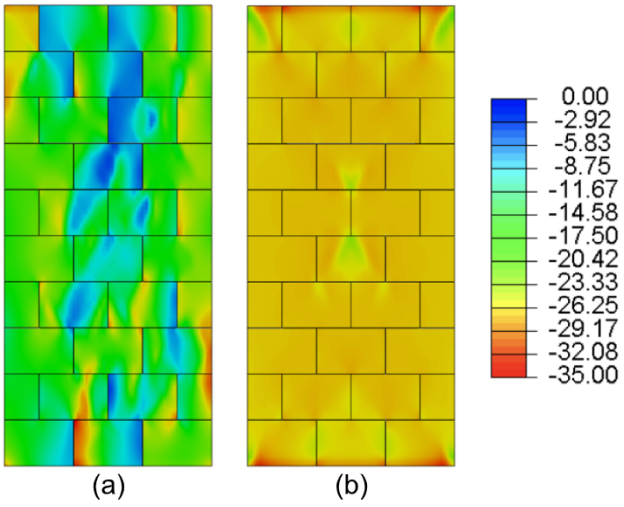

Fig. 22. Minimum principal stress (in MPa) distribution in the masonry due to applied peak compressive force: a) model with varying joint thicknesses; b) model with uniform joint thickness.

arising from the manufacturing process [40–42]. Due to these differences, results obtained from the joint closure experiments cannot be applied to the large-scale masonry. Therefore, identifying the joint parameters becomes a complex task. Two approaches can be used to represent dry joints to numerically simulate such experiments on the mortarless masonry at the meso-level. The dry joints can be modelled randomly with varying joint thickness, or joints can be modelled with a uniform average thickness. For this numerical simulation, both approaches are compared. Fig. 19a shows the random selection of joint thicknesses at the bed joints ranging from 0.119 mm (value acquired from the dry joint experiment in the previous section) to 0.419 mm (maximum joint thickness acquired by Oliveira et al. [6]). The stress at the half-joint closure, $\sigma_{1/2}$ and parameter n are kept the same for all the joint thicknesses, 1.2 MPa and 0.8, respectively. For the head joints, a constant value of 0.119 mm was adopted. For the numerical model with uniform joint thickness, an average value of 0.27 mm was selected, as shown in Fig. 19b. When dealing with mortarless masonry, only the friction coefficient (or friction angle) needs to be identified for the shear behaviour. For this purpose, a friction coefficient value of 0.598 was chosen based on the experiments performed by Oliveira et al. [6] on alumina-spinel bricks. For the normal behaviour, joint closure relations are provided in a tabular form as a surface-to-surface contact for interface in Abaqus due to the lack of commercially available constitutive models for such applications. This interface model allows to input stress-overclosure relationships (for the normal behaviour) that can be computed by the exponential model at regular intervals and it also allows to define friction behaviour with a value for friction coefficient (for the shear behaviour).

The numerical model was constructed by modelling full bricks of size $150 \times 140 \times 100$ mm^3 (length $\times$ width $\times$ height) and half bricks of size $75 \times 140 \times 100$ mm^3. The brick units were discretized with 8-node solid elements (C3D8R elements) with a size of $10 \times 10 \times 10$ mm^3. The dry joints were modelled as the surface-to-surface contact interfaces. The final mesh is composed of 69,100 elements for bricks and 43,568 interface elements. The numerical model is shown in Fig. 20a. Regarding boundary conditions, the model is considered fixed at the base, and the load is applied as increasing displacement in the vertical direction from the top face of the wall as shown in the Fig. 20a. To represent the effect of the loading beam, the loading was applied using a rigid plate with its all three rotational degrees of freedom restrained. For the top face of the wall no restraints were applied.

The results obtained from this numerical analysis are presented in Fig. 20b in terms of stress displacement profile. The vertical displacement profiles are derived from the relative displacement between the top and bottom brick layers. From the figure, it can be observed that the numerical results are in good agreement with the experimental results. The numerical results show a similar joint closing behaviour at the lower stress level as the experimental results. Once the joints are closed, the model with uniform joint thickness shows a linear stiffness of the masonry wall that is similar to the material stiffness. In comparison, the model with varying joint thicknesses shows linear behaviour with reduced stiffness. This reduction is primarily due to material damage due to uneven local boundary conditions presented by the varying joint thicknesses. Consequently, the model with varying joint thickness fails with peak stress of 16.4 MPa, which is closer to the values observed experimentally. In the case of the model with uniform average joint thickness, the model fails at a much higher value of 27.34 MPa, due to uniform joints that do not allow stress concentration in the bricks.

Fig. 21, shows the distribution of displacement in the vertical direction for the numerical models considering varying joint thicknesses and uniform joint thickness at the peak applied compressive force. From the figure, it can be observed that for the model with varying joint thicknesses (Fig. 21a), the displacements observed are primarily caused by the joint closure and brick units undergo only minor deformations. However, the vertical displacement is not uniform for all the brick layers. In contrast, in the model with the uniform joint thickness (Fig. 21b), the vertical displacement is uniform for all the brick layers. This difference between both approaches is expected due to the difference in the distribution of the joint thicknesses.

Fig. 22, shows the distribution of minimum principal stress (compressive stress) in the masonry wall for both modelling approaches at the peak applied compressive force. For the model with varying joint thicknesses (Fig. 22a), a non-uniform distribution of stresses can be observed. Such distribution is due to uneven joint thickness, which restricts the direct load transfer from one layer of brick to other. Therefore, the bricks undergoing significant stresses will yield first, which ultimately reduces the observed global stiffness of the masonry. However, in the case of the model with the uniform joint thickness (Fig. 22b), an essentially uniform distribution of the stresses can be observed. Such behaviour is expected due to uniform joint thickness, allowing the uniform transfer of forces from one layer of brick to another. Nevertheless, a high concentration of stresses can be observed at the top and bottom faces of the masonry due to global boundary conditions.

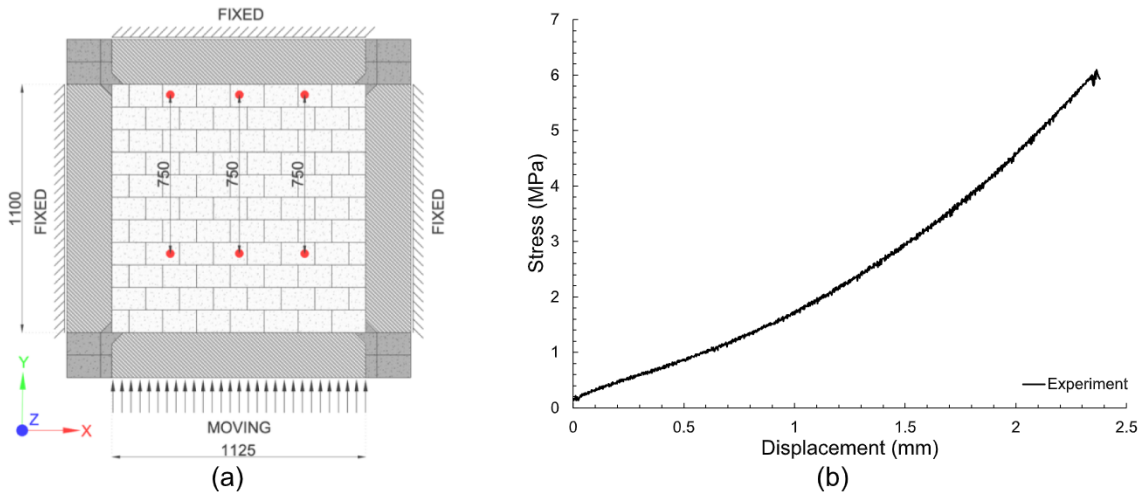

Fig. 23. Uniaxial compression experiment on mortarless masonry at high temperature: a) graphical representation of the experimental setup; b) stress-displacement results obtained from experiment (adapted from Oliveira [11]).

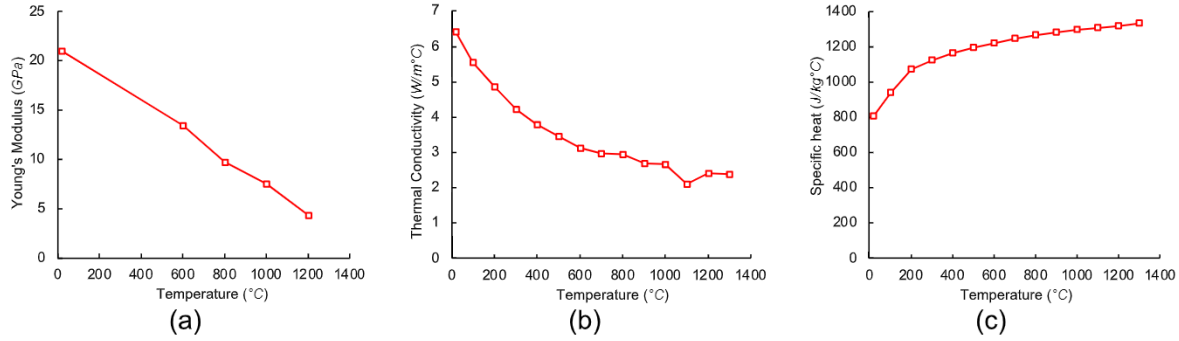

Fig. 24. Thermal and mechanical properties of alumina-spinel bricks: a) Young's modulus; b) thermal conductivity [31]; c) specific heat [31].

5.2. Numerical modelling at high temperature

To validate the proposed model at high temperatures, a new model was developed using a similar meso-modelling approach. This model intends to replicate an experimental test performed within the scope of the ATHOR project. This experiment was performed at 1200 °C by applying uniaxial compressive force perpendicular to the bed joint direction (as shown in Fig. 23a). This test was performed as a preliminary test at the Technology Centre Leoben (TCL) of RHI-Magnesita, Austria, under the framework of the ATHOR project [11]. In this experiment, the brick units (150 × 100 × 140 mm^3) of alumina-spinel material were laid on a layer of insulation bricks. Thermal load was applied with electrical heating elements arranged near the hot face (HF) of the masonry. For the duration of thermal loads, masonry unit was free to expand. Once the desirable temperature was achieved near the HF, the loading was applied. During the load application, three sides of the rigid blocks were fixed, as shown in Fig. 23a. Relative displacement between two points (red circles marked in Fig. 23a) were gathered during the experiments at three different locations. The average displacements obtained from this experiment are presented in Fig. 23b.

The numerical model was constructed using the same approach as discussed in the previous section. However, in this simulation, only the elastic properties of the brick were considered due to low level of stress applied. Temperature dependent material properties of alumina-spinel is shown in Fig. 24. For Young's modulus (Fig. 24a), material stiffness evaluated in section 4.1 and 4.2 were considered. Thermal conductivity and specific heat of the material are shown in Fig. 24b and c [31]. The coefficient of thermal expansion of the material is considered as 8.87 × 10^{-6} K^{-1} [35]. The friction coefficient between alumina-spinel bricks has been characterized by Oliveira et al. [6] at different temperatures and reported in Table 7.

Table 7
Friction coefficient values for dry joints at different temperatures [6].

Temperature (°C)	20	300	600	900
Friction coefficient (-)	0.60	0.50	0.51	0.53

The meso model of the masonry is shown in Fig. 25. The X direction (1125 mm) is the direction normal to head joints, while the Y direction (1100 mm) is normal to bed joints. The four ceramic plates and the insulation layer (ground) of the test setup have been modelled as rigid plates. The masonry units were meshed with 3D hexahedron elements with 35 × 35 × 35 mm^3 size elements. Frictional interactions between the contact surfaces of the wall and the fixed, moving rigid plates and the ground were considered with a friction coefficient of 0.5 [1]. At hot face of the wall, no restraints were applied as it was the case with the experimental test.

For the simulation, coupled thermal–mechanical analysis was performed. For the thermal loads, average values of the observed temperatures at hot face (HF) and cold face (CF) through thermocouples are used. Fig. 26a presents the temperature distribution in the masonry wall at the load application (i.e., 29.75 h). Time variations at the HF and CF of the masonry wall along with experimental observations is shown in Fig. 26b. During the thermal load application (i.e., till 29.75 h) the masonry wall was free to expand. During the mechanical load application, relevant boundary conditions were applied, as presented in Fig. 25.

For the normal dry joint behaviour, uniform joint thickness at the

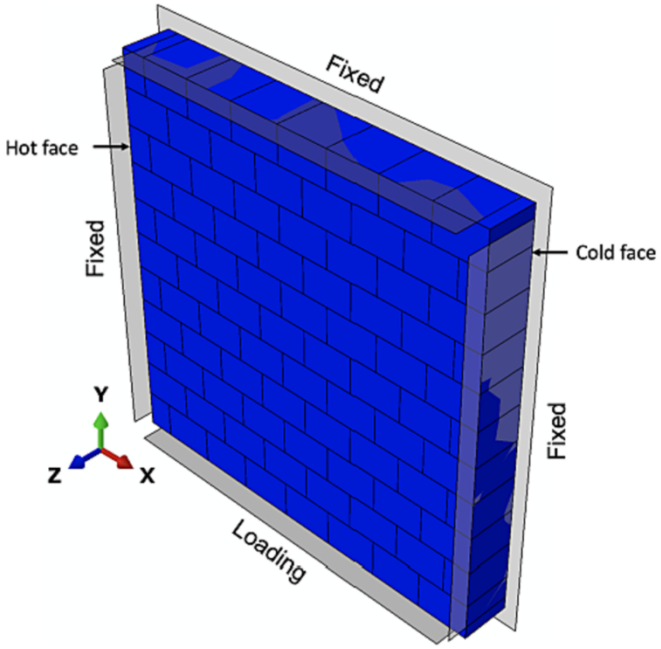

Fig. 25. Meso-model for the high temperature uniaxial compressive test simulation presenting individual brick units and rigid plates.

bed and head joints are assumed. This was assumed considering similarity in the global behaviour during initial loading stage (i.e., till 6 MPa) between both approaches (considering uniform and non-uniform joint thicknesses) in section 5.1 (Fig. 20b). Furthermore, two cases are considered in this numerical simulation, joint closure relationship observed at the ambient temperature and at 1200 °C. As discussed in the previous section, the joint thickness varies in a large-scale masonry unit, therefore a uniform joint thickness of 0.22 mm was derived for this experiment by calibrating it with experimental results. The joint closure behaviour for both cases is shown in Fig. 27. The stress at the half-joint closure, $\sigma_{1/2}$ is 1.3 MPa for ambient temperature and 0.6 MPa at 1200 °C (as derived from the joint closure experiments). The value of parameter n is 0.8 for both cases.

Fig. 28 presents the results obtained from numerical simulations and experiments. The numerical results indicate that both cases are in good agreement with experimental results at low stress levels (up to 3 MPa). However, at 6 MPa, the difference between the numerical result, *Num - AT* and experiment is relatively large. The error obtained for displacements between the numerical and experimental result is 1.60 % and 7.67 % for the *Num - HT* and *Num - AT*, respectively. The difference observed for the global stiffness is 8.71 % and 13.26 % for the *Num - HT* and *Num - AT*, respectively. This difference is due to the joint closure behaviour. As observed in Fig. 27, for 6 MPa, the joints are open at ambient temperature, in contrast to 1200 °C, where the joints are fully closed. Considering the low level of force applied in this experiment, the difference between numerical results for both cases is not much. However, at high force levels, this difference would increase.

The minimum principal stress distribution in the masonry wall at the end of the loading (i.e. 6 MPa of applied stress) is shown in Fig. 29a. The results are shown for the numerical simulation considering the joint behaviour of 1200 °C. From the figure, high concentration of stress can be observed near the hot face of the masonry (around 9 MPa) compared to cold face (around 2 MPa). This difference is due to thermal expansion of the brick units. The units will expand more under higher temperature, therefore, the thermal gradient within the bricks (Fig. 26a) causes hot face to expand more compared to the cold face. This ultimately results in reduced joint thickness at HF and relatively large joint thickness at the CF. Therefore, as the load is applied on the masonry, HF will experience higher loads until the joints near the CF comes into contact.

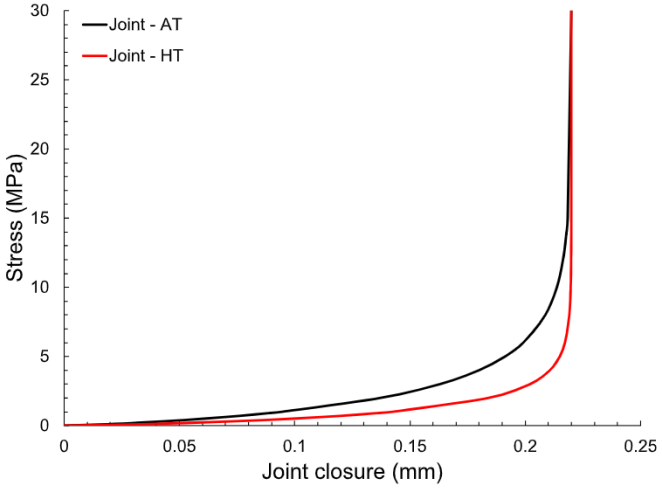

Fig. 27. Joint closure behaviour adopted in the numerical simulation at high temperature. Joint - AT, represents behaviour at ambient temperature and Joint - HT, at 1200 °C.

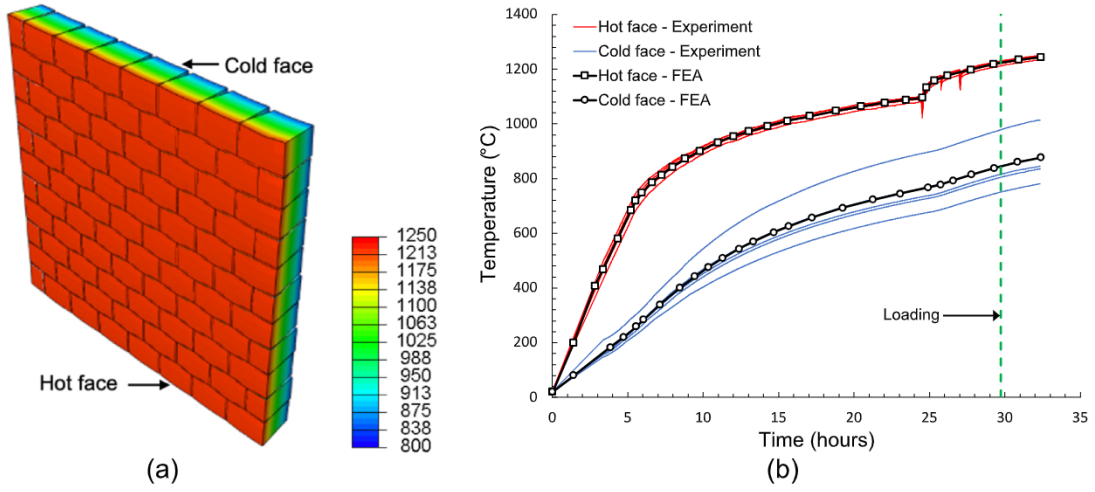

Fig. 26. Thermomechanical analysis: a) temperature distribution in the deformed masonry wall during load application (deformations magnified by 50 times); b) time variations of the cold and hot face temperatures during heating and mechanical testing, experimental and numerical results.

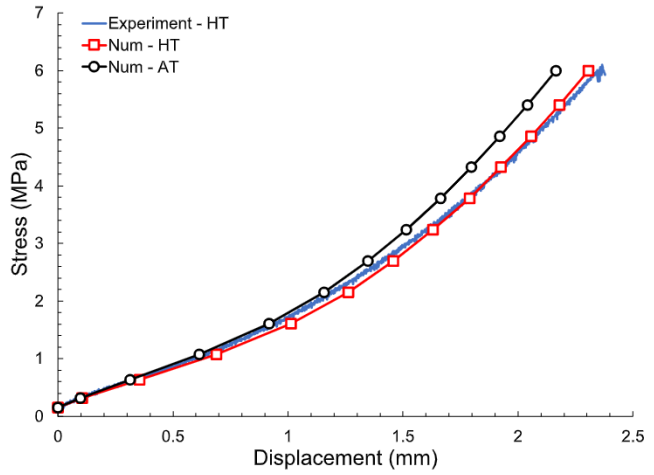

Fig. 28. Stress-displacement profile from experiment and numerical simulations. Experiment - HT shows experimental results obtained during uniaxial compressive test at high temperature. Num - HT indicates a model with joint thicknesses behaviour at 1200 °C. Num - AT shows the model with joint thickness behaviour at ambient temperature.

Displacement distribution normal to the bed joints is shown in Fig. 29b. From the figure, it can be observed that at the applied thermal and mechanical loads, the brick units experience minor deformation compared to the joint as observed in previous section. Given the difference in material stiffness at HF and CF and thermal expansion of the material, displacement difference between HF and CF is expected, however, this difference is much lower compared to the global displacement of the wall and therefore it cannot be observed in the Figure.

6. Conclusions

Mortarless masonry poses a unique complexity in terms of dry joints. The behaviour of these joints depends on many factors, such as surface roughness, surface unevenness, manufacturing tolerances and unevenness arising from the construction of such masonry. In modern practice, mortarless masonry is widely used in an industrial environment where it is subjected to high operating temperatures. Therefore, identifying the joint behaviour at high temperatures and a suitable mathematical model that represents the behaviour is crucial for numerical simulations.

This paper reviews the available mathematical models for the dry joints and compares those models with the experimental results at a wide range of temperatures for the alumina-spinel material. For this purpose, the exponential model [12], hyperbolic model [26], power-law model [28] and model proposed by Thanoon et al. [25] are reviewed and compared with experimental results at ambient temperature, 600 °C, 800 °C, 1000 °C and 1200 °C. A mathematical model should be such that it can best represent the joint behaviour at all temperature ranges and should require a parameter that is relatively easy to identify. From the analysis of the experimental results, the exponential model is selected for further consideration due to the better fit it provided for the experimental results compared to hyperbolic model due to additional degree of freedom, and its ease in defining the material parameters.

Joint thickness and stress values identified by the exponential model show that the overall joint thickness reduced with an increase in temperature, from 0.119 mm at ambient temperature to 0.041 mm at 1200 °C. This reduction is primarily due to the thermal expansion of the material (similar to the observation made by Andreev et al. [13]). Moreover, the stress required for half joint closure also reduces with an increase in temperature due to decreasing material stiffness as the temperature increases. Furthermore, the analysis of joint reloading shows a reduction of 40 % in the joint thickness due to surface damage, at various tested temperatures.

Results obtained from the cyclic loading and subsequent inverse analysis via analytical model show that the joint thickness only reduces after the first loading cycle. For subsequent loading cycles, joint thickness does not change. Additionally, an increase in the stress required for half joint closure is observed after the fifth loading cycle. The 3D measurements of the joint surfaces before and after the loading shows that, for this material surface profile does not change much for the level of force applied.

Furthermore, finite element analysis was carried out using a meso-modelling approach to check the exponential model's efficacy at larger scales. The numerical investigation at ambient temperature is carried out considering two cases, random distribution of varying joint thicknesses and a uniform average joint thickness. Results obtained for both cases show a good agreement with the experimental results. These results further show that the exponential model is able to provide good results with relative ease as the parameters required can be easily identified from the experimental results. Moreover, numerical investigation carried out for high temperature experiments shows the importance of the joint closure relationships at various temperatures. The joint closure behaviour obtained for the ambient temperature can provide better results at low stress levels but at higher stress levels, the numerical results diverge from the actual global behaviour of the masonry at higher temperature. Therefore, for numerical simulations at various temperature levels, the joint closure behaviour at those temperature

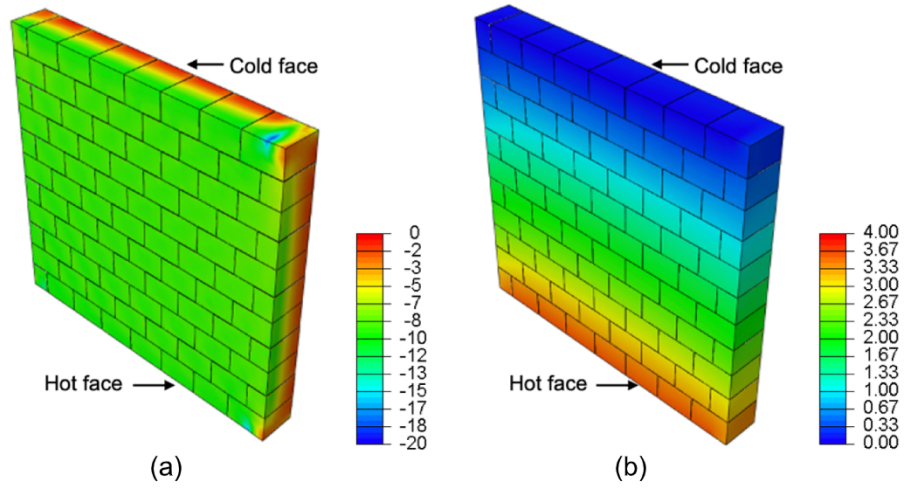

Fig. 29. Thermomechanical analysis results: a) minimum principal stress distribution (MPa); b) in-plane displacement distribution along the Y direction (mm).

should be used.

Currently, the FEA software does not have any commercially available constitutive models that can be used to represent all the aspects of the dry joint behaviour, such as cyclic joint closing and opening behaviour, the capability of providing different parameters at different temperatures. At present, most FEA software allows only to input a tabular form of stress/stiffness – overclosure relations. To better represent the dry joint behaviour for a mortarless masonry under the thermomechanical loading, a user-supplied subroutine is required for the interface, which can consider the different aspects of the joint behaviour mentioned in this work. The exponential model is one such model based on which a user-supplied subroutine can be made, as it is easier to use, and it requires parameters that can be identified from the experimental results. Such model will allow definition of joints with physical properties such as joint thickness and stress levels. Moreover, it will also allow to define these properties at various temperature levels so that the evolution of joint behaviour with temperature can be better represented. This is paramount for the appropriate representation of dry joint refractory masonry at the meso-level but can be also relevant for the development of homogenised models, as the joint behaviour highlighted within this work should be considered when developing such models.

Declaration of Competing Interest

The authors declare that they have no known competing financial interests or personal relationships that could have appeared to influence the work reported in this paper.

Data availability

Data will be made available on request.

Acknowledgement

This work was supported by the funding scheme of the European Commission, Marie Skłodowska-Curie Actions Innovative Training Networks in the frame of the project ATHOR - Advanced THermo-mechanical multiscale mOdelling of Refractory linings 764987 Grant. The first, third and sixth authors acknowledge the partial funding by FCT / MCTES through national funds (PIDDAC) under the R&D Unit Institute for Sustainability and Innovation in Structural Engineering (ISISE), under reference UIDB/04029/2020.

References

[1] Nguyen TMHH, Blond E, Gasser A, Prietl T. Mechanical homogenisation of masonry wall without mortar. European Journal of Mechanics-A/Solids 2009;28 (3):535–44. https://doi.org/10.1016/j.euromechsol.2008.12.003.

[2] Ali M, Sayet T, Gasser A, Blond E. Computational Homogenization of Elastic-Viscoplastic Refractory Masonry with Dry Joints. Int J Mech Sci Apr. 2021;196: 106275. https://doi.org/10.1016/j.ijmecsci.2021.106275.

[3] Samadi S, Jin S, Harmuth H. Combined damaged elasticity and creep modeling of ceramics with wedge splitting tests. Ceram Int Sep. 2021;47(18):25846–53. https://doi.org/10.1016/J.CERAMINT.2021.05.315.

[4] Blond E, Nguyen AK, de Bilbao E, Sayet T, Batakis A. Thermo-chemo-mechanical modeling of refractory behavior in service: Key points and new developments. Int J Appl Ceram Technol Aug. 2020;17(4):1693–700. https://doi.org/10.1111/IJAC.13499.

[5] Oliveira RLG, Rodrigues JPC, Pereira JM, Lourenço PB, Marschall HU. Thermomechanical behaviour of refractory dry-stacked masonry walls under uniaxial compression. Eng Struct 2020;240(December):2021. https://doi.org/10.1016/j.engstruct.2021.112361.

[6] Oliveira RLG, Rodrigues JPC, Pereira JM, Lourenço PB, Ulrich Marschall H. Normal and tangential behaviour of dry joints in refractory masonry. Eng Struct 2021;243: 112600. https://doi.org/10.1016/j.engstruct.2021.112600.

[7] Ali, M., T. Sayet, A. Gasser, and E. Blond, "Transient Thermo-Mechanical Analysis of Steel Ladle Refractory Linings Using Mechanical Homogenization Approach," Ceramics 2020, Vol. 3, Pages 171-189, vol. 3, no. 2, pp. 171–188, Apr. 2020, doi: 10.3390/ceramics3020016.

[8] Jin S, Gruber D, Harmuth H, Frechette MH. Thermomechanical steel ladle simulation including a Mohr-Coulomb plasticity failure model. RHI Bull 2012;1: 39–43.

[9] Andreev K, Harmuth H. FEM simulation of the thermo-mechanical behaviour and failure of refractories - A case study. J Mater Process Technol 2003;143–144(1): 72–7. https://doi.org/10.1016/S0924-0136(03)00322-4.

[10] Ali, M., "Nonlinear thermomechanical modelling of refractory masonry Linings," PhD thesis ,University of Orléans - France, 2021.

[11] Oliveira, R., "Experimental and numerical thermomechanical characterization of refractory masonaries," PhD thesis, University of Coimbra - Portugal, 2022.

[12] Malama B, Kulatilake PHSW. Models for normal fracture deformation under compressive loading. Int J Rock Mech Min Sci Sep. 2003;40(6):893–901. https://doi.org/10.1016/S1365-1609(03)00071-6.

[13] Andreev K, Sinnema S, Rekik A, Allaoui S, Blond E, Gasser A. Compressive behaviour of dry joints in refractory ceramic masonry. Constr Build Mater Sep. 2012;34:402–8. https://doi.org/10.1016/J.CONBUILDMAT.2012.02.024.

[14] Blond, E., G. Alain, L. Matthieu, and J.-L. Daniel, "Modelling of joint effect in refractory structures," 2010.

[15] Gasser A, Terny-Rebeyrotte K, Boisse P. Modelling of joint effects on refractory lining behaviour. Proceedings of the Institution of Mechanical Engineers, Part L: Journal of Materials: Design and Applications 2004;218(1):19–28. https://doi.org/10.1243/146442004322849881.

[16] Allaoui S, Rekik A, Gasser A, Blond E, Andreev K. Digital Image Correlation measurements of mortarless joint closure in refractory masonries. Constr Build Mater Feb. 2018;162:334–44. https://doi.org/10.1016/J.CONBUILDMAT.2017.12.055.

[17] Prakash PR, Azenha M, Pereira JM, Lourenço PB, Lourenco P. Finite element based micro modelling of masonry walls subjected to fire exposure: Framework validation and structural implications. Eng Struct Jun. 2020;213:110545. https://doi.org/10.1016/j.engstruct.2020.110545.

[18] Lourenço, P. B., "Computational strategies for masonry constructions," Ph. D. thesis, Delft Univ. Press, Delft, The Netherlands, 1996.

[19] Lourenco PB, Silva LC. Computational applications in masonry structures: from the meso-scale to the super-large/super-complex. Int J Multiscale Comput Eng 2020;18 (1):1–30.

[20] Zucchini A, Lourenço PB. A micro-mechanical model for the homogenisation of masonry. Int J Solids Struct 2002;39(12):3233–55.

[21] Lourenço PB, Rots JG, Blaauwendraad J. Two approaches for the analysis of masonry structures: micro and macro-modeling. HERON 1995;40(4):1995.

[22] Nodargi NA, Intrigila C, Bisegna P. A variational-based fixed-point algorithm for the limit analysis of dry-masonry block structures with non-associative Coulomb friction. Int J Mech Sci Oct. 2019;161–162:105078. https://doi.org/10.1016/J.IJMECSCI.2019.105078.

[23] Cascini L, Gagliardo R, Portioli F. LiABlock_3D: A Software Tool for Collapse Mechanism Analysis of Historic Masonry Structures. International Journal of Architectural Heritage Jan. 2020;14(1):75–94. https://doi.org/10.1080/15583058.2018.1509155.

[24] Naik P, Bhowmik T, Menon A. Estimating joint stiffness and friction parameters for dry stone masonry constructions. International Journal of Masonry Research and Innovation 2021;6:232–54. https://doi.org/10.1504/IJMRI.2020.10033088.

[25] Thanoon WAM, Alwathaf AH, Noorzaei J, Jaafar MS, Abdulkadir MR. Finite element analysis of interlocking mortarless hollow block masonry prism. Comput Struct Mar. 2008;86(6):520–8. https://doi.org/10.1016/J.COMPSTRUC.2007.05.022.

[26] Goodman RE, Taylor RL, Brekke TL. A Model for the Mechanics of Jointed Rock. Journal of the Soil Mechanics and Foundations Division May 1968;94(3):637–59. https://doi.org/10.1061/JSFEAQ.0001133.

[27] Bandis SC, Lumsden AC, Barton NR. Fundamentals of rock joint deformation. International Journal of Rock Mechanics and Mining Sciences & Geomechanics Abstracts Dec. 1983;20(6):249–68. https://doi.org/10.1016/0148-9062(83)90595-8.

[28] Swan G. Determination of stiffness and other joint properties from roughness measurements. Rock Mech Rock Engng 1983;16(1):19–38.

[29] Barton N, Bandis S, Bakhtar K. Strength, deformation and conductivity coupling of rock joints. International Journal of Rock Mechanics and Mining Sciences & Geomechanics Abstracts Jun. 1985;22(3):121–40. https://doi.org/10.1016/0148-9062(85)93227-9.

[30] Brosnan, D. A., "Alumina-Silica brick," in *Refractories Handbook*, 1st ed., C. A. Schacht, Ed. CRC Press, 2004, pp. 79–108. doi: 10.1201/9780203026328.

[31] Vitiello D. Thermo-physical properties of insulating refractory materials. Université de Limoges 2021.

[32] Samadi S, Jin S, Gruber D, Harmuth H, Schachner S. Statistical study of compressive creep parameters of an alumina spinel refractory. Ceram Int 2020;46 (10):14662–8. https://doi.org/10.1016/j.ceramint.2020.02.267.

[33] Schacht CA. Refractory lining: Thermomechanical design and applications. Mechanical Engineering 1995.

[34] En,. 993–5:2000, "Methods of test for dense shaped refractory products - Part 5: Determination of cold crushing strength". European Committee for Standardisation 2000.

[35] Kaczmarek R. Mechanical characterization of refractory materials. Université de Limoges; 2021. Ph.D thesis.

[36] Smith M. ABAQUS/Standard User's Manual, Version 2019. United States: Dassault Systèmes Simulia Corp; 2019.

[37] Lee J, Fenves GL. Plastic-Damage Model for Cyclic Loading of Concrete Structures. J Eng Mech Aug. 1998;124(8):892–900. https://doi.org/10.1061/(ASCE)0733-9399(1998)124:8(892).

[38] Lubliner J, Oliver J, Oller S, Oñate E. A plastic-damage model for concrete. Int J Solids Struct Jan. 1989;25(3):299–326. https://doi.org/10.1016/0020-7683(89)90050-4.

[39] Kaczmarek, R. *et al.*, "Thermomechanical behaviour of an alumina spinel refractory for steel ladle applications," Oct. 2019. [Online]. Available: https://hal-unilim.archives-ouvertes.fr/hal-02533698.

[40] Zahra T, Dhanasekar M. Characterisation and strategies for mitigation of the contact surface unevenness in dry-stack masonry. Constr Build Mater Apr. 2018; 169:612–28. https://doi.org/10.1016/j.conbuildmat.2018.03.002.

[41] Chewe Ngapeya GG, Waldmann D, Scholzen F. Impact of the height imperfections of masonry blocks on the load bearing capacity of dry-stack masonry walls. Constr Build Mater 2018;165:898–913.

[42] Agaajani, S., "Development and Investigation of a New Dry-Stacked Wall System," PhD thesis, University of Luxembourg, 2015.